OXFORD

Human Molecular Genetics, 2017, Vol. 26, No. 1 1–18

doi: 10.1093/hmg/ddw363
Advance Access Publication Date: 25 October 2016
Original Article

ORIGINAL ARTICLE

Leucine-rich repeat kinase 2 exacerbates neuronal cytotoxicity through phosphorylation of histone deacetylase 3 and histone deacetylation

Kyung Ah Han[1], Woo Hyun Shin[1], Sungyeon Jung[1], Wongi Seol[2], Hyemyung Seo[3], CheMyong Ko[4] and Kwang Chul Chung[1,*]

[1]Department of Systems Biology, College of Life Science and Biotechnology, Yonsei University, Seoul, Republic of Korea, [2]InAm Neuroscience Research Center, Sanbon Medical Center, College of Medicine, Wonkwang University, Gunpo-si, Gyeonggi-do, Republic of Korea, [3]Department of Molecular and Life Sciences, College of Science and Technology, Hanyang University, Ansan-si, Gyeonggi-do, Republic of Korea and [4]Department of Comparative Biosciences, College of Veterinary Medicine, University of Illinois at Urbana-Champaign, Urbana, IL, USA

*To whom correspondence should be addressed at: Kwang Chul Chung, Department of Systems Biology, College of Life Science and Biotechnology, Yonsei University, Yonsei-ro 50, Seodaemun-gu, Seoul 120-749, Republic of Korea. Tel: +82-2-2123-2653; Fax: +82-2-312-5657; Email: kchung@yonsei.ac.kr

Abstract

Parkinson's disease (PD) is characterized by slow, progressive degeneration of dopaminergic neurons in the substantia nigra. The cause of neuronal death in PD is largely unknown, but several genetic loci, including *leucine-rich repeat kinase 2* (*LRRK2*), have been identified. LRRK2 has guanosine triphosphatase (GTPase) and kinase activities, and mutations in *LRRK2* are the major cause of autosomal-dominant familial PD. Histone deacetylases (HDACs) remove acetyl groups from lysine residues on histone tails, promoting transcriptional repression via condensation of chromatin. Here, we demonstrate that LRRK2 binds to and directly phosphorylates HDAC3 at Ser-424, thereby stimulating HDAC activity. Specifically, LRRK2 promoted the deacetylation of Lys-5 and Lys-12 on histone H4, causing repression of gene transcription. Moreover, LRRK2 stimulated nuclear translocation of HDAC3 via the phoshorylation of karyopherin subunit α2 and α6. HDAC3 phosphorylation and its nuclear translocation were increased in response to 6-hydroxydopamine (6-OHDA) treatment. LRRK2 also inhibited myocyte-specific enhancer factor 2D activity, which is required for neuronal survival. LRRK2 ultimately promoted 6-OHDA-induced cell death via positive modulation of HDAC3. These findings suggest that LRRK2 affects epigenetic histone modification and neuronal survival by facilitating HDAC3 activity and regulating its localization.

Introduction

Parkinson's disease (PD) is a progressive neurodegenerative disorder characterized by the death of dopaminergic neurons in the substantia nigra pars compacta (1) and the presence of abnormal protein aggregates in the cytosol known as Lewy bodies (LBs) (2). While the aetiology of PD remains largely unknown, several genetic loci have been implicated in the pathogenesis of familial PD. *Leucine-rich repeat kinase 2* (*LRRK2*) is a genetic factor known to cause the autosomal-dominant form of PD (3). *LRRK2* encodes a large, multi-domain protein with kinase, guanosine triphosphatase (GTPase) and protein–protein interaction

Received: October 11, 2016. **Revised:** October 11, 2016. **Accepted:** October 18, 2016

domains (LRR, COR and WD40). *LRRK2* mutants have been known to cause neural degeneration (4). For example, the most common G2019S mutation increases the kinase activity of LRRK2, promoting cellular toxicity (5,6). The LRRK2-R1441C mutation decreases its GTPase and increases its kinase activities (6,7), but there are conflicting results regarding this kinase-modifying effect (3). A number of LRRK2 substrates involved in diverse signalling pathways have been identified. For example, LRRK2 participates in vesicle trafficking, mitochondria function, microtubule dynamics, immunity and protein translational regulation through interaction with various proteins (8). Despite its role in different cellular pathways, the molecular mechanism of LRRK2-induced neurodegeneration is still unclear.

Histone deacetylases (HDACs) remove acetyl groups from lysine residues on histone tails, promoting transcriptional repression via condensation of chromatin (9). There are 18 different mammalian HDACs, which can be divided into four classes based on sequence similarities (10). HDAC3 is a class I HDAC, and is distinguishable from other class I HDACs (HDAC1, HDAC2 and HDAC8) by its localization (10). Chromosome region maintenance 1 (CRM1) mediates HDAC3 movement between the nucleus and the cytoplasm (11). Thus, HDAC3 is found in the nucleus, cytoplasm and plasma membrane, whereas HDACs 1 and 2 predominantly localize in the nucleus (10,12).

Histones H2, H3 and H4 are the typical substrates of HDAC3 (13). H2-K5, H4-K5 and H4-K12 are completely deacetylated by HDAC3, but H3, H2B, H4-K8 and H4-K16 are only partially deacetylated (13). Furthermore, HDAC3 mainly targets and deacetylates three lysine residues of H4 at its K5, K8 and K12 sites (14). Consistent with these findings, *HDAC3* deletion leads to increased acetylation of some H3 and H4 tails, including H4-K5 and H4-K12 (15,16). HDAC3 also deacetylates various non-histone targets, such as Myocyte-specific enhancer factor 2D (MEF2D) (17), NF-κB (18), retinoblastoma protein (19) and p53 (20).

Recent studies have demonstrated that HDAC3 is involved in neurotoxic process. For example, knockdown of *Had-3*, a nematode homolog of *HDAC3*, reduces poly-Q-Huntingtin toxicity, while overexpression of *Had-3* restores neurotoxicity induced by poly-Q-huntingtin in the *Caenorhabditis elegans* model of Huntington's disease (21). Moreover, HDAC3 interacts with HDAC1, a well-known molecular switch between neuronal survival and death, promoting neuronal death (22). Interestingly, a number of kinases regulate the activity and/or cytotoxicity of HDAC3. For example, casein kinase 2, PTEN-induced putative kinase 1 (PINK1) and DNA-dependent protein kinase phosphorylate HDAC3 and enhance its enzymatic activity (20,23,24). Glycogen synthase kinase-3β (GSK-3β) also regulates the neurotoxic function of HDAC3 through its kinase activity (25).

Despite currently limited knowledge about the substrates of LRRK2 and their biological effects, it remains necessary to identify and characterize other targets of LRRK2 and their physiological functions for a complete understanding of its neurotoxic mechanisms and contribution to the pathogenesis of PD. To identify additional substrates and/or regulators of LRRK2, we performed yeast two-hybrid screenings using wild-type LRRK2 as bait. After screening of a human fetal brain cDNA library, we identified HDAC3 as a novel interaction partner of LRRK2. Based on these findings, we investigated a possible functional link between LRRK2 and HDAC3 during neuronal death. Here, we report that HDAC3 is a novel substrate of LRRK2 in mammalian neuronal cells. We further demonstrate that LRRK2 facilitates cytotoxicity through phosphorylation of HDAC3.

Results

LRRK2 interacts and co-localizes with HDAC3

To determine whether LRRK2 and HDAC3 interact in mammalian cells, co-immunoprecipitation experiments were performed. After HEK293 cells were transfected with Myc-LRRK2 and/or Flag-HDAC3, total cell lysates were immunoprecipitated with an anti-Myc antibody. Immunoblotting of anti-Myc immunocomplexes with an anti-Flag antibody indicated an interaction between ectopically expressed LRRK2 and HDAC3 (Fig. 1A). Co-immunoprecipitation of cell lysates in the reverse order further confirmed the interaction between LRRK2 and HDAC3 (Fig. 1B).

Next, to determine whether LRRK2 co-localizes with HDAC3, immunocytochemical analyses were performed. After HEK293 cells were transfected with Myc-LRRK2 and Flag-HDAC3 constructs, immunostaining with anti-Myc and anti-Flag antibodies showed that LRRK2 and HDAC3 co-localize mainly in the cytosol (Fig. 1C). Consistent with the previous finding (10), HDAC3 was present in equal proportions in the nucleus and cytosol.

In vitro GST pull-down assays further demonstrated a direct interaction between LRRK2 and HDAC3 (Fig. 1D). To address the possibility that these results were artifact of DNA transfection, we further tested whether endogenous LRRK2 binds to endogenous HDAC3 in neuroblastoma SH-SY5Y cells. Co-immunoprecipitation of cell lysates was performed using anti-HDAC3 or anti-LRRK2 antibodies, followed by immunoblotting with anti-LRRK2 or anti-HDAC3 antibodies. Endogenous LRRK2 was found to bind endogenous HDAC3 in SH-SY5Y cells (Fig. 1E). Confocal microscopy revealed that endogenous LRRK2 co-localized with endogenous HDAC3 in SH-SY5Y cells (Fig. 1F). Moreover, immunoprecipitation using whole brain and kidney lysates from 8-week-old mice further indicated that there is an interaction between LRRK2 and HDAC3 (Fig. 1G). Collectively, these results suggest that LRRK2 specifically binds HDAC3 in mammalian cells.

LRRK2 specifically phosphorylates HDAC3 at ser-424

To address whether LRRK2 directly phosphorylates HDAC3, *in vitro* kinase assays were performed using recombinant GST-fused HDAC3 as a substrate, and Myc-tagged LRRK2-WT or LRRK2-KD mutant was immunoprecipitated from HEK293 cell lysates. Autoradiography of the reaction products showed that wild-type LRRK2, but not its kinase-deficient form, phosphorylates HDAC3 *in vitro* (Fig. 2A). In addition, LRRK2 has no effect on GST alone as a control (Supplementary Material, Fig. 1). We also observed that phosphorylation of endogenous HDAC3 at serine residue(s) is increased by LRRK2 overexpression in SH-SY5Y cells (Fig. 2B).

We then assessed the migration of HDAC3 in the presence or absence of LRRK2 in a phos-tag gel. SDS-polyacrylamide gel containing phos-tag specifically retards the migration of phosphorylated proteins, which are visualized as slow-migrating bands, compared with non-phosphorylated control counterparts. HEK293 cells were transfected with Flag-tagged HDAC3 alone, or with either Myc-tagged wild-type LRRK2 or its kinase-dead mutant (LRRK2-KD). A slow-migration band corresponding to phosphorylated HDAC3 was observed in the presence of wild-type LRRK2 on the phos-tag gel; however, this band was markedly diminished in the presence of LRRK2-KD (Fig. 2C). Collectively, these results suggest that HDAC3 serves as a substrate for LRRK2.

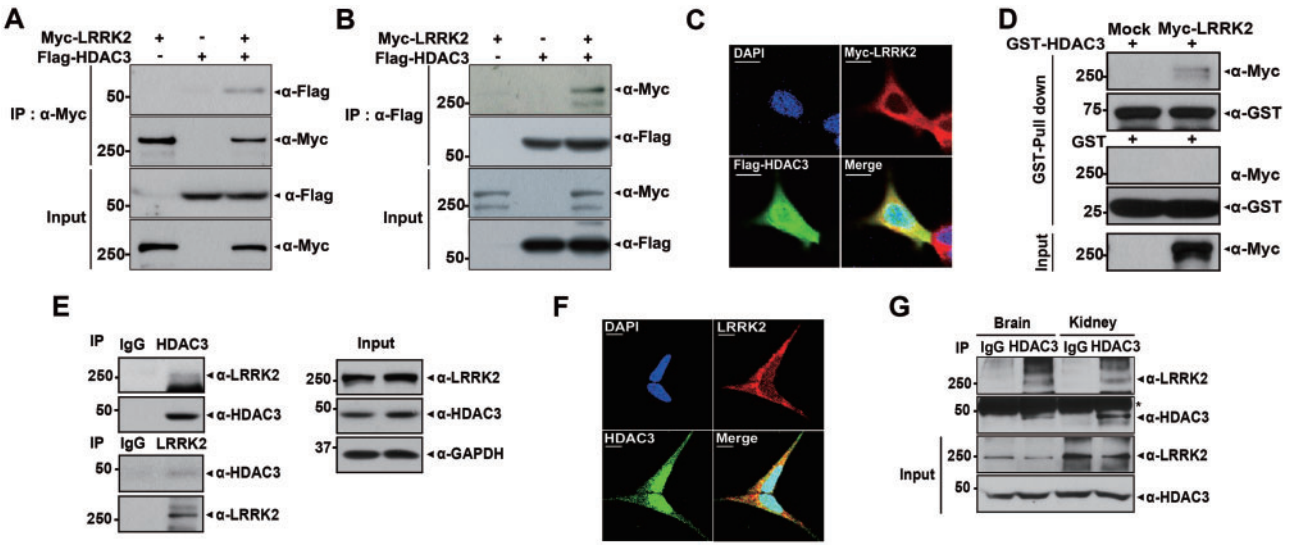

Figure 1. LRRK2 binds to HDAC3. (A,B) HEK293 cells were transfected for 24 h with plasmids encoding Myc-LRRK2 and/or Flag-HDAC3, and co-immunoprecipitation assays were performed with anti-Myc (A) or anti-Flag (B) antibodies, as indicated. Immunocomplexes were analysed using anti-Flag **(A)** or anti-Myc (B) antibodies. The expression of transiently-transfected proteins in cell lysates were determined by western blotting with anti-Myc or anti-Flag antibodies. **(C)** HEK293 cells were transfected for 24 h with plasmids encoding Myc-LRRK2 and Flag-HDAC3. Where specified, cells were fixed, permeabilized, and stained with either anti-Myc antibody followed by TRITC-conjugated secondary antibody or anti-Flag antibody followed by FITC-conjugated secondary antibody. Nuclei were counterstained with DAPI. Immunostained cells were analysed using confocal microscopy (LSM 510 META, Carl Zeiss, scale bars: 10 μm). **(D)** GST pull-down assays were performed using GST-HDAC3-immobilized glutathione-sepharose and HEK293 cell lysates were prepared after a 24 h transfection with Myc-LRRK2. Bound complexes were analysed by western blotting with anti-Myc antibody and GST served as a negative control. Purification of GST-fused HDAC3 and the presence of Myc-LRRK2 in cell extracts were confirmed by western blotting with anti-GST or anti-Myc antibodies, respectively. **(E)** Where indicated, immunoprecipitation of neuroblastoma SH-SY5Y cell lysates was performed using anti-HDAC3 or anti-LRRK2 antibodies, followed by immunoblotting with anti-LRRK2 or anti-HDAC3 antibodies. As a negative control, cell lysates were immunoprecipitated with pre-immune IgG (IgG). The expression of LRRK2 and HDAC3 in cell extracts was determined by immunoblotting with anti-LRRK2 or anti-HDAC3 antibodies. GAPDH served as a loading control. **(F)** SH-SY5Y cells were fixed, permeabilized, and labelled with anti-LRRK2 and anti-HDAC3 antibodies. Cells were then stained with TRITC- and FITC-conjugated secondary antibodies. Nuclei were counterstained with DAPI. Immunostained preparations were examined with a confocal microscope (scale bars: 10 μm). **(G)** Immunoprecipitation of mouse brain or kidney lysates was performed using an anti-HDAC3 antibody, followed by immunoblotting with anti-LRRK2 antibody. As a control, cell lysates were immunoprecipitated with pre-immune IgG (IgG). The expression of LRRK2 and HDAC3 in tissue lysates was determined by immunoblotting with anti-LRRK2 or anti-HDAC3 antibodies.

We next investigated the effects of two PD-linked mutants (LRRK2-G2019S and LRRK2-R1441C) on HDAC3 phosphorylation. Both mutants, particularly LRRK2-G2019S, increased levels of phosphorylated HDAC3 by approximately 1.5 fold (Fig. 2D).

To determine which region(s) of HDAC3 is phosphorylated by LRRK2, we performed *in vitro* kinase assays using GST-fused HDAC3 deletion mutants. After DNA transfection with Myc-LRRK2-WT for 24 h, HEK293 cell lysates were incubated with bacterially-expressed GST-HDAC3 deletion mutants. Anti-Myc immunocomplexes phosphorylated multiple recombinant HDAC3 truncation mutants, which all contained the C-terminal NLS domain, spanning the amino acids 313-428 (Fig. 3A and B). This effect was not observed with the HDAC3 fragment lacking the NLS domain (Fig. 3B). As the NLS region contains twelve Ser/Thr residues, we sought to identify which among them is/are targeted by LRRK2. Four GST-HDAC3 fragments with triple point mutations at twelve Ser/Thr residues were tested as targets for LRRK2 phosphorylation. Among them, the HDAC3 mutant with alanine substitutions at T390/S405/S424 exhibited greatly reduced levels of phosphorylation by LRRK2 (Fig. 3C), but the other three mutants were unaffected.

We next generated three GST-HDAC3 mutants with point mutations at the T390, S405, or S424 position; *in vitro* kinase assays were performed. The GST-HDAC3 mutant with a single point mutation at S424A exhibited no HDAC3 phosphorylation, whereas the other two HDAC3 mutants (T390A and S405A) did not show any change in LRRK2-mediated phosphorylation (Fig. 3D). These results indicate that LRRK2 specifically phosphorylates HDAC3 at Ser-424. These results were corroborated by assays utilizing two PD-linked mutants (LRRK2-G2019S and LRRK2-R1441C). Although these two mutants enhance LRRK2 kinase activity, co-transfection with the HDAC3-S424A mutant completely abolished phosphorylation of HDAC3 (Fig. 3E).

Next, we tested whether LRRK2 phosphorylates HDAC3 at Ser-424 residue *in vivo*. Immunoblotting of SH-SY5Y cell lysates with an anti-phospho-antibody specific to HDAC3-S424 showed that wild-type LRRK2 overexpression causes an increase in its endogenous level by approximately 1.9-fold (Fig. 3F). This effect was not seen in cells transfected with the LRRK2-KD mutant (Fig. 3F). Furthermore, the phosphorylated HDAC3 level at S424 was dramatically increased by two PD-linked LRRK2 mutants (Fig. 3G).

We further verified the effect of LRRK2 on the phosphorylation of HDAC3-S424 by employing *LRRK2*-siRNA. While the efficiency of siRNA against *LRRK2* was validated by immunoblot analyses (Fig. 3H), HDAC3 phosphorylation was significantly reduced in cells transfected with *LRRK2*-siRNA, compared with nonspecific siRNA (Fig. 3I). We then examined the effect of LRRK2 deletion on the phosphorylation of HDAC3-S424. Western blotting of cell lysates with phospho-HDAC3-S424-specific antiserum revealed that levels were significantly decreased in *LRRK2* -/- MEFs, compared with control *LRRK2* +/+ MEFs (Fig. 3J).

To determine the physiological relevance of LRRK2-mediated phosphorylation of HDAC3 in neuronal cell death, we

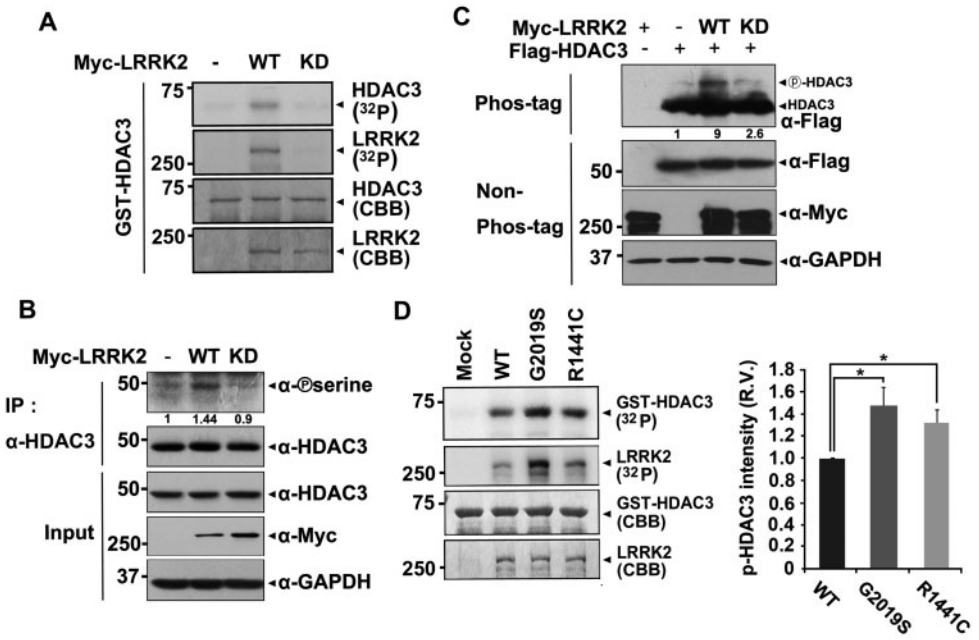

Figure 2. LRRK2 directly phosphorylates HDAC3. **(A)** HEK293 cells were transfected for 24 h with Myc-tagged LRRK2-WT or LRRK2-KD. Cells were immunoprecipitated with anti-Myc IgG, and the samples were incubated for 15 min with recombinant GST-HDAC3 and [γ-^{32}P]. The reaction products were separated by SDS-PAGE and autoradiograms were acquired. **(B)** SH-SY5Y cells were transfected for 24 h with Myc-tagged LRRK2-WT or LRRK2-KD. Immunoprecipitation of cell lysates was performed using an anti-HDAC3 antibody, followed by immunoblotting with an anti-phospho-Ser antibody. Transiently-expressed Myc-LRRK2 and endogenous HDAC3 proteins were identified by western blotting with anti-Myc or anti-HDAC3 antibodies. GAPDH served as a loading control. **(C)** HEK293 cells were transfected for 24 h with plasmids encoding Flag-tagged HDAC3, Myc-tagged LRRK2-WT, or LRRK2-KD alone or in combination, as indicated. Cell lysates were separated on a phos-tag gel, followed by western blotting using an anti-Flag antibody (phos-tag). The expression of transiently-transfected proteins in cell lysates was determined by separation by SDS-PAGE and western blotting using anti-Myc or anti-Flag antibodies (non-phos-tag). GAPDH served as a loading control. **(D)** HEK293 cells were transfected with plasmids encoding Myc-tagged LRRK2-WT, LRRK2-G2019S, or LRRK2-R1441C. Cell lysates were immunoprecipitated using an anti-Myc IgG, and incubated for 15 min with recombinant GST-tagged wild-type HDAC3 and [γ-^{32}P]. The reaction products were separated by SDS-PAGE and autoradiograms were acquired (left panel). Data are representative of three independent experiments. Relative phosphorylated HDAC3 protein levels were quantified using MultiGauge V. 3.1 program ($n = 3$; * $P < 0.05$; right panel).

investigated the effects on LRRK2 activity and HDAC3 phosphorylation of exposure of *LRRK2* +/+ and *LRRK2* -/- MEFs to 6-OHDA. Stereotaxic injection of the neurotoxin 6-OHDA into the substantia nigra region of mid-brain is widely used to lesion dopaminergic pathways and generate experimental mouse models for PD. After cells were treated with 6-OHDA for 12 h, immunoblotting of cell lysates demonstrated that treatment of *LRRK2* +/+ MEFs with 6-OHDA enhances LRRK2 kinase activity. Moreover, the level of phosphorylated HDAC3-Ser-424 was greatly increased in *LRRK2* +/+ versus *LRRK2* -/- MEFs (Fig. 3K). In addition, the amount of phosphorylated HDAC3 bands was increased by overexpressed LRRK2-WT or LRRK2-GS, which was further enhanced under 6-OHDA treatment (Fig. 3L).

Collectively, these data suggest that LRRK2 specifically phosphorylates HDAC3 at its Ser-424 residue and that treatment with 6-OHDA stimulates LRRK2 kinase activity.

LRRK2-mediated phosphorylation of HDAC3 increases its deacetylase activity

Based on previous reports that the deacetylase activity of HDAC3 is positively regulated by phosphorylation at Ser-424 (20,23), we next investigated the effect of LRRK2 on HDAC3 activity. After HEK293 cells were transfected with Flag-tagged wild-type HDAC3 and/or Myc-tagged LRRK2-WT, LRRK2-KD, or the LRRK2-G2019S mutant, the HDAC3 activity of anti-Flag immunocomplexes was analysed by measuring the luminescence of the luminogenic peptide substrate resulting from HDAC-mediated deacetylation. Results showed that the overexpression of wild-type LRRK2 enhances HDAC3 deacetylase activity, with the LRRK2-G2019S mutant further enhancing this activity (Fig. 4A). The kinase-inactive LRRK2 mutant did not have this effect (Fig. 4A).

HDAC3 forms a tight complex with the silencing mediator for retinoid and thyroid hormone receptors (SMRT) and nuclear receptor corepressor (N-CoR), which act as transcriptional co-regulatory factors; proper association is necessary for efficient deacetylation of substrate histones by HDAC3 (26). Based on these findings, we then examined whether LRRK2 promotes formation of a transcriptional co-repressor complex that include these two proteins. Dopaminergic neuroblastoma SH-SY5Y cells were transfected with Myc-tagged LRRK2-WT or LRRK2-KD, and cell lysates were immunoprecipitated with an anti-HDAC3 antibody. Immunoblotting of the samples with anti-SMRT or anti-N-CoR antibodies revealed that wild-type LRRK2 increases the amount of HDAC3 complexed with SMRT/N-CoR, but this effect was not observed in cells transfected with the LRRK2-KD mutant (Fig. 4B and C). To verify the plausible role of HDAC3 phosphorylation in the formation of HDAC3/SMRT/N-CoR complex, we examined the effect of phosphorylation-mimetic HDAC3-S424E and phosphorylation-defective HDAC3-S424A mutant on it. Comparing with LRRK2-WT, these two mutants had no apparent effect on the complex formation (Fig. 4D and E). These results suggest that LRRK2 kinase activity is necessary, not only for positive modulation of HDAC3 activity, but also for the enhanced formation of transcriptional co-regulatory

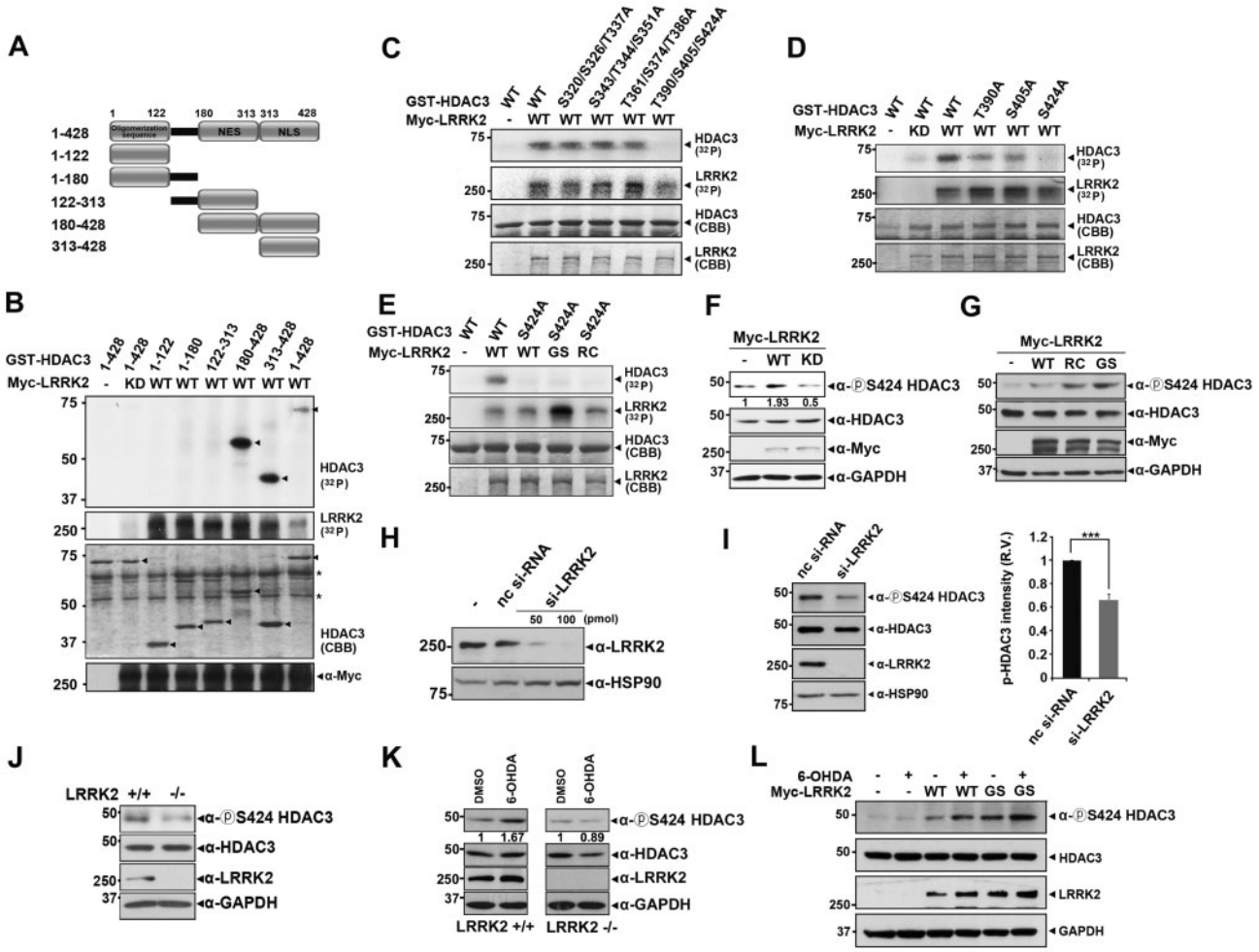

Figure 3. LRRK2 phosphorylates HDAC3 at Ser-424 with 6-OHDA treatment. **(A)** Schematic representation of HDAC3 and its truncated mutants. **(B)** HEK293 cells were transfected for 24 h with Myc-tagged LRRK2-WT or LRRK2-KD. Cell lysates were immunoprecipitated using anti-Myc antibodies, and incubated for 15 min with recombinant GST-HDAC3-WT or its truncated mutants and [γ-^{32}P]. The reaction products were separated by SDS-PAGE and autoradiograms were acquired **(B–E)**. **(C)** HEK293 cells were transfected for 24 h with Myc-LRRK2-WT, and cell lysates were immunoprecipitated with anti-Myc antiserum. Immunocomplexes were incubated for 15 min with recombinant GST-tagged HDAC3-WT or mutants containing various triple point mutations (HDAC3-S320/S326/T337A, HDAC3-S343/T344/S351A, HDAC3-T361/S374/T386A, or HDAC3-T390/S405/S424A) with [γ-^{32}P]. **(D)** HEK293 cells were transfected with Myc-tagged LRRK2-WT or LRRK2-KD. Where specified, anti-Myc immunocomplexes were prepared using an anti-Myc antibody and incubated for 15 min with either purified GST-HDAC3-WT or its single point mutant proteins (T390A, S405A, or S424A) and [γ-^{32}P]. **(E)** HEK293 cells were transfected with Myc-tagged LRRK2-WT, LRRK2-G2019S, or LRRK2-R1441C. Target proteins were immunoprecipitated using anti-Myc antibodies, followed by incubation for 15 min with recombinant GST-tagged HDAC3-WT or the HDAC3-S424A mutant with [γ-^{32}P]. **(F)** SH-SY5Y cells were transfected for 24 h with Myc-tagged LRRK2-WT or LRRK2-KD. Immunoblotting of cell lysates was performed using an anti-phospho-Ser424-HDAC3 antibody. Expression of exogenous Myc-LRRK2 and endogenous HDAC3 proteins was detected using anti-Myc or anti-HDAC3 antibodies. **(G)** HEK293 cells were transfected for 24 h with Myc-tagged LRRK2-WT, LRRK2-G2019S or LRRK2-R1441C. Immunoblotting of cell lysates was performed using anti-phospho-HDAC3 (S424) antibody. Levels of exogenous Myc-LRRK2 and endogenous HDAC3 proteins were detected using anti-Myc or anti-HDAC3 antibodies. **(H)** SH-SY5Y cells were either mock-transfected or transfected for 48 h with non-specific control siRNA (nc; 100 pM) or the indicated concentrations of *LRRK2*-siRNA (si-*LRRK2*). Cell lysates were immunoblotted with anti-LRRK2 antibody. **(I)** SH-SY5Y cells were transfected for 48 h with nc siRNA (100 pM) or *LRRK2-siRNA* (100 pM). Cell lysates were immunoblotted with anti-phospho-Ser424-HDAC3, anti-HDAC3, or anti-LRRK2 antibodies (left panel). Relative phosphorylated HDAC3 protein level was quantified using the MultiGauge V. 3.1 program ($n = 4$; *** $P < 0.001$; right panel). **(J)** *LRRK2* +/+ and *LRRK2* -/- MEF lysates were probed using an anti-phospho-HDAC3-S424 antibody. Levels of endogenous LRRK2 and HDAC3 proteins were detected by immunoblotting using their respective antibodies. **(K)** After *LRRK2* +/+ and *LRRK2* -/- MEFs were treated for 12 h with 100 μM 6-OHDA, cell lysates were separated by SDS-PAGE. Immunoblotting was performed using anti-phospho- HDAC3-S424 antibody. **(L)** SH-SY5Y cells were transfected for 24 h with Myc-tagged LRRK2-WT or LRRK2-G2019S, and then left untreated or treated for 12 h with 6-OHDA (100 μM). Immunoblotting of cell lysates was performed with anti-phospho-Ser424-HDAC3 antibody. Levels of exogenous Myc-LRRK2 and endogenous HDAC3 proteins were detected using anti-Myc or anti-HDAC3 antibodies.

complexes that include HDAC3. However, the formation of the HDAC3/SMRT/N-CoR complex is not affected by HDAC3 phosphorylation.

LRRK2 promotes nuclear translocation of HDAC3

HDAC3 is known to shuttle between the nucleus and cytoplasm, but the mechanism underlying this nuclear translocation is largely unknown. Moreover, HDAC3-containing SMRT and N-CoR complexes are usually found in the nucleus. Based on these findings, we next examined whether interaction between HDAC3 and LRRK2 affects the intracellular localization and/or transport of HDAC3. After SH-SY5Y cells were transfected with Myc-tagged LRRK2-WT or the LRRK2-KD mutant, cytoplasmic and nuclear fractions were prepared via cell fractionation. Immunoblotting of each fraction with an anti-HDAC3 antibody

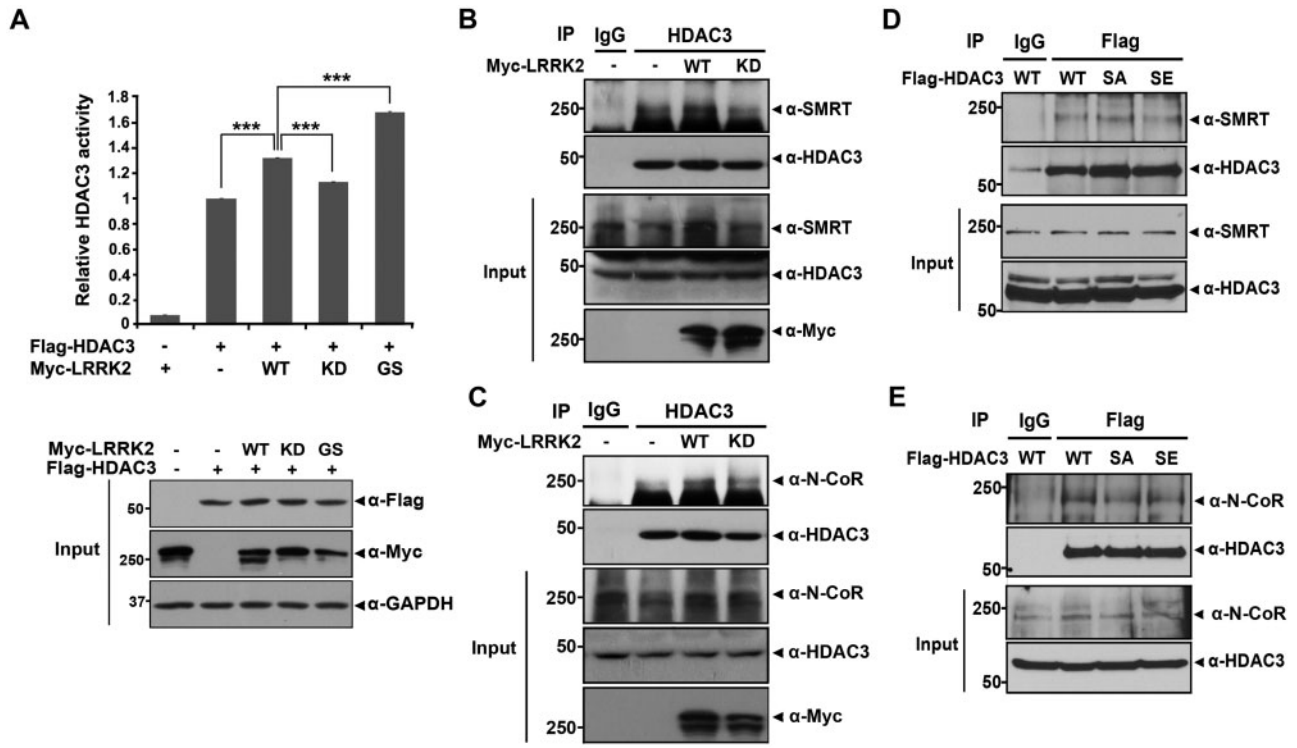

Figure 4. LRRK2 enhances HDAC3 activity. **(A)** HEK293 cells were transfected for 24 h with plasmids encoding either Flag-tagged HDAC3-WT alone or with Myc-tagged LRRK2-WT, LRRK2-KD, or LRRK2-GS2019S (LRRK2-GS). Cells were lysed with 1% NP-40 lysis buffer and target proteins immunoprecipitated using anti-Flag antibodies. HDAC3 activity in anti-Flag immunocomplexes was determined using HDAC assay kit. All transfections were normalized to parental expression vectors, and data are expressed as the mean ± S.E.M of three independent experiments ($n = 3$; *** $P < 0.001$). **(B,C)** SH-SY5Y cells were mock-transfected or transfected for 24 h with Myc-tagged LRRK2-WT or LRRK2-KD. Immunoprecipitation of target proteins in cell lysates was performed using IgG or HDAC3 antibodies, followed by immunoblotting with anti-SMRT **(B)** or anti-N-CoR antibodies **(C)**, as indicated. **(D,E)** HEK293 cells were mock-transfected or transfected for 24 h with Flag-tagged HDAC3-WT, HDAC3-S424A or HDAC3-S424E. Immunoprecipitation of cell lysates was performed using IgG or Flag antibodies, followed by immunoblotting with anti-SMRT **(D)** or anti-N-CoR antibodies **(E)**, as indicated.

revealed that overexpression of LRRK2-WT, but not LRRK2-KD, increases nuclear HDAC3 levels, accompanied by a corresponding decrease in cytosolic HDAC3 levels (Fig. 5A). These results suggest that LRRK2 induces nuclear translocation of HDAC3 in a kinase-dependent manner.

To confirm these results, we evaluated the localization of HDAC3 in MEFs derived from *LRRK2* -/- and control *LRRK2* +/+ mice. Immunoblotting with an anti-HDAC3 IgG indicated that there were greater levels of endogenous HDAC3 in the cytosol versus the nucleus in *LRRK2* -/- MEFs. In contrast, HDAC3 was much enriched in the nuclear fraction in *LRRK2* +/+ MEFs compared with the cytoplasmic fraction (Fig. 5B). Next, we reconstituted *LRRK2* -/- MEFs with wild-type LRRK2 or the LRRK2-G2019S or LRRK2-R1441C mutant and examined the effect on subcellular localization of HDAC3. Immunoblotting of the two fractions showed that in the presence of LRRK2-WT, accumulation of HDAC3 in the cytosol was greatly reduced and a significant amount of HDAC3 translocated into the nucleus. Moreover, reconstitution with two PD-linked LRRK2 mutants enhanced HDAC3 nuclear translocation compared with wild-type LRRK2 (Fig. 5C).

We next examined the effects of 6-OHDA treatment on HDAC3 nuclear translocation. *LRRK2* +/+ and *LRRK2* -/- MEFs were treated with 6-OHDA for 12 h before cell fractionation. The level of cytoplasmic HDAC3 decreased, while levels of nuclear HDAC3 increased in *LRRK2* +/+ MEFs. Treatment of *LRRK2* -/- MEFs with 6-OHDA did not affect levels of cytosolic HDAC3 and did not induce any significant nuclear translocation of HDAC3 (Fig. 5D). LRRK2-G2019S mutant also induced the translocation of HDAC3 into the nucleus more dramatically than LRRK2-WT in SH-SY5Y cells (Fig. 5E). Moreover, 6-OHDA treatment accelerated the effect of LRRK2-G2019S mutant (Fig. 5E). These results suggest that LRRK2 mediates nuclear translocation of HDAC3, which is further enhanced by treatment with 6-OHDA. These findings were further supported by the immunocytochemical analyses, confirming that LRRK2-WT and its two PD-linked promote the nuclear translocation of HDAC3 (Fig. 5F).

We then addressed whether the phosphorylation of HDAC3-S424 promotes nuclear translocation of HDAC3. We examined the intracellular localization of Flag-tagged HDAC3 mutants with single or multiple point mutations at three Ser/Thr residues in the NLS domain. Both the HDAC3-S424A and HDAC3-T390/S405/S424A mutants were found to translocate into the nucleus to an extent equal to wild-type HDAC3 (Fig. 6A). Additionally, the intracellular localization of HDAC3 was unaffected by the phospho-mimetic S424E mutation (Fig. 6B). These results suggest that phosphorylation at Ser-424 has no effect on HDAC3 nuclear translocation.

These results alternatively indicate that sites other than Thr-390, Ser-405 and Ser-424 serve as targets for phosphorylation to induce HDAC3 nuclear translocation. Thus, we additionally investigated the nuclear transport of other HDAC3 mutants with single or double point mutations in other NLS domains (S320/S326A, T337A, S343/344A, S351A, S361A, S374A, T386A, T390A, S405A, or S424A). The nuclear and cytoplasmic distributions of HDAC3 were similar among these mutants (Fig. 6C).

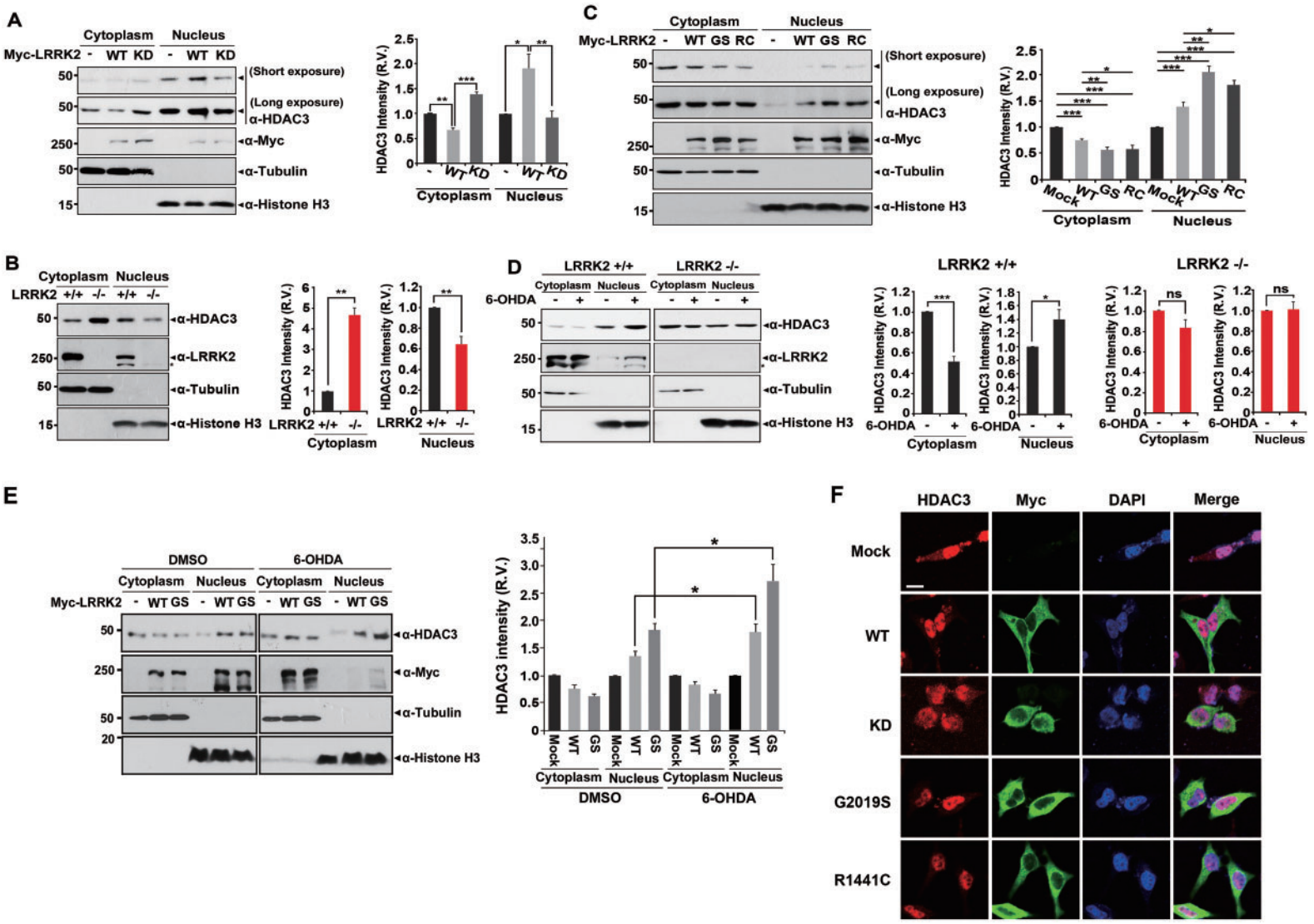

Figure 5. LRRK2 induces nuclear translocation of HDAC3, which is increased by 6-OHDA treatment. **(A)** SH-SY5Y cells were transfected for 36 h with Myc-tagged LRRK2-WT or LRRK2-KD and fractionated into cytoplasmic and nuclear fractions. Each fraction was immunoblotted with anti-HDAC3 or anti-Myc antibodies. The purity of each fraction was confirmed by immunoblotting with α-tubulin (cytoplasmic marker) or histone H3 (nuclear marker) antibodies **(A-E)**. Data are representative of three to five independent experiments. Relative endogenous HDAC3 protein levels in the cytoplasm or nucleus were quantified using the MultiGauge V 3.1 program (* $P < 0.05$; ** $P < 0.01$; *** $P < 0.001$, n.s., not significant; **A-E**). **(B)** *LRRK2* +/+ and *LRRK2* -/- MEFs were fractionated into cytoplasmic and nuclear fractions. Immunoblotting of each fraction were performed with anti-LRRK2 or anti-HDAC3 antibodies. **(C)** *LRRK2* -/- MEF cells were transfected for 24 h with Myc-tagged LRRK2-WT, LRRK2-G2019S, or LRRK2-R1441C. Cells were fractionated into cytoplasmic and nuclear fractions. Immunoblotting of each fraction was performed using anti-Myc or ant-HDAC3 antibodies. **(D)** *LRRK2* +/+ and *LRRK2* -/- MEFs were treated for 12 h with DMSO or 100 μM 6-OHDA, and fractionated into cytoplasmic and nuclear fractions. Each fraction sample was immunoblotted with anti-HDAC3 or anti-LRRK2 antibodies. **(E)** SH-SY5Y cells were transfected for 36 h with Myc-tagged LRRK2-WT or LRRK2-G2019S, treated for 12 h with DMSO or 6-OHDA (100 μM), and then fractionated into cytoplasmic and nuclear fractions. Each fraction sample was immunoblotted with anti-HDAC3 or anti-LRRK2 antibodies. **(F)** SH-SY5Y cells were transfected for 24 h with Flag-HDAC3 alone or together with Myc-tagged LRRK2-WT, LRRK2-KD, LRRK2-G2019S, or LRRK2-R1441C. Cells were fixed, permeabilized, and stained with either anti-Myc antibody followed by FITC-conjugated secondary antibody or anti-HDAC3 antibody followed by TRITC-conjugated secondary antibody. Nuclei were counterstained with DAPI. Immunostained cells were analysed using confocal microscopy (LSM 700 META, Carl Zeiss, scale bars: 10 μm)

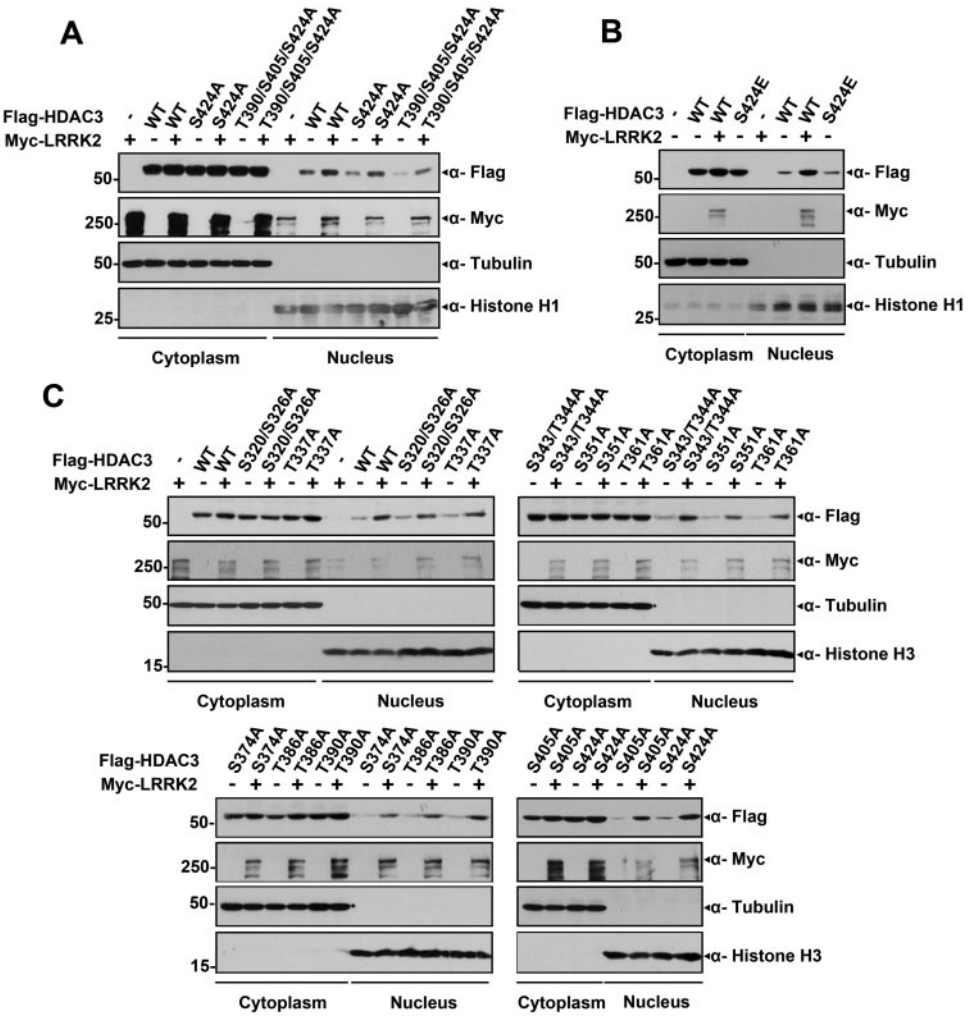

Figure 6. Phosphorylation of HDAC3 at Ser-424 or the NLS domain is not required for its nuclear translocation. **(A)** Where specified, HEK293 cells were transfected for 24 h with plasmids encoding Flag-tagged HDAC3-WT, its single (HDAC3-S424A) or triple (HDAC3-T390/S405/S424A) point mutant, or Myc-tagged wild-type LRRK2 alone or in combination. Cells were fractionated into cytoplasmic and nuclear fractions **(A–C)**. Each fraction was resolved by SDS-PAGE and analysed by western blotting with anti-Flag or anti-Myc antibodies. The purity of each fraction was confirmed by immunoblotting with α-tubulin (cytoplasmic marker) or histone H1 or H3 (nuclear marker) antibodies **(A–C)**. **(B)** HEK293 cells were transfected with plasmids encoding Flag-tagged HDAC3-WT, its phosphorylation-mimetic mutant (HDAC3-S424E), or Myc-tagged LRRK2-WT alone or in combination, as indicated. **(C)** HEK293 cells were transfected for 24 h with plasmids encoding Flag-tagged HDAC3-WT, its various single or double point mutants, or Myc-tagged LRRK2-WT alone or in combination, as indicated.

Collectively, these data suggest that LRRK2 positively regulates HDAC3 nuclear translocation, but this modulation is not dependent upon direct phosphorylation of HDAC3-S424.

Although efficient shuttling between the cytosol and nucleus is important for the histone-modifying actions of and transcriptional co-repression induced by HDAC3, the underlying mechanism remains unclear. Macromolecules and proteins commonly interact with karyopherins for proper translocation into the nucleus. Karyopherins have two subunits, karyopherin-α and karyopherin-β, which shuttle cytosolic proteins into the nucleus by detecting and binding the NLS. Karyopherin-α first recognizes the NLS of the cargo protein; karyopherin-β then interacts with the N-terminus of karyopherin-α, and the cargo complex is imported into the nucleus. Thus, we next examined whether HDAC3 interacts with karyopherin-α subtypes. HEK293 cells were co-transfected with plasmids encoding Flag-tagged HDAC3 and a HA-tagged karyopherin-α subtype protein (KPNA-1, -2, -3, -4, or -6). Co-immunoprecipitation of anti-Flag immunocomplexes with anti-HA antiserum demonstrated that HDAC3 specifically interacts with KPNA-2 and -6 (Supplementary Material, Fig. S2D and E). HDAC3 did not bind to KPNA-1, -3, or -4 (Supplementary Material, Fig. S2A–C). Furthermore, when cells were co-transfected with either Myc-tagged LRRK2-WT or LRRK2-KD, wild-type LRRK2 promoted binding of HDAC3 to KPNA-2 and KPNA-6, while the kinase-dead mutant failed to affect their binding (Fig. 7A and B). We then examined whether LRRK2 directly phosphorylates KPNA2 and 6. Co-immunoprecipitation assays of anti-KPNA2 and 6 immunocomplexes with anti-phospho-Ser antibody revealed that the phosphorylation of KPNA2 and 6 is increased by LRRK2-WT, but not by LRRK2-KD (Fig. 7C and D), implying that KPNA 2/6, as the novel substrates of LRRK2, could mediate the nuclear translocation of HDAC3, possibly through phosphorylation.

Collectively, the overall results suggest that karyopherin-α2 and -α6 mediate the nuclear translocation of HDAC3, and LRRK2 kinase activity enhances their binding affinities.

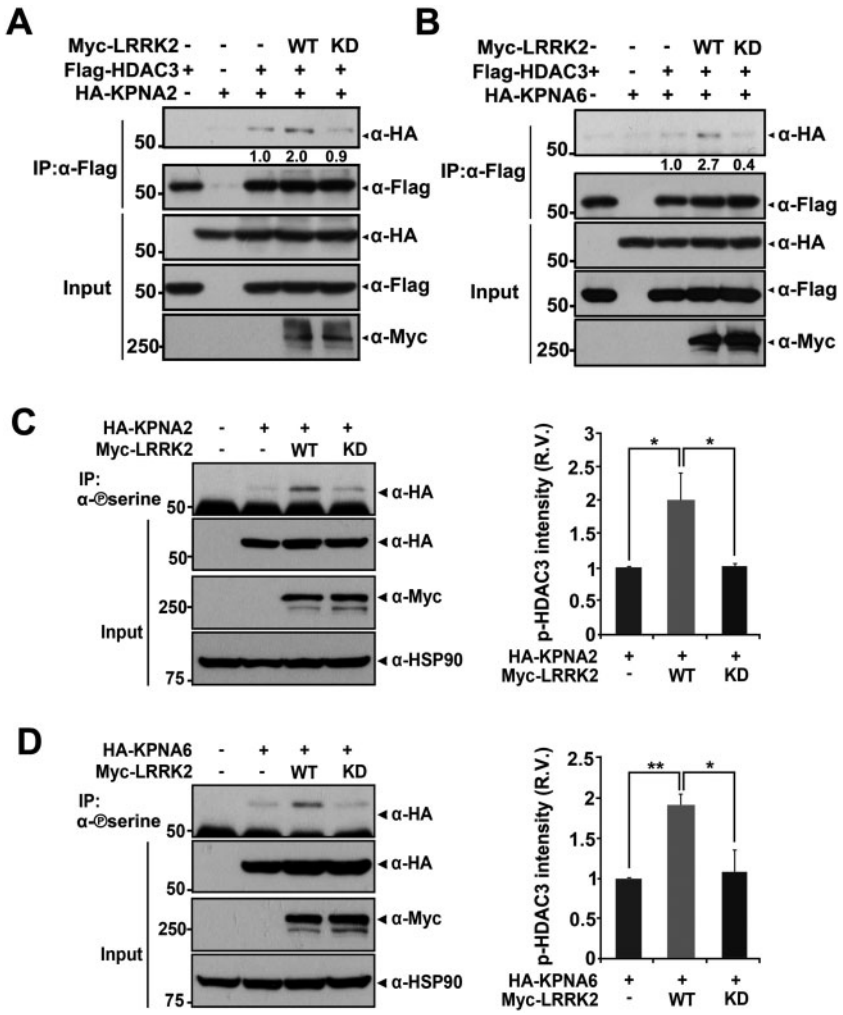

Figure 7. LRRK2 increases the interaction between HDAC3 and KPNA2/6. **(A,B)** Where specified, HEK293 cells were transfected for 24 h with plasmids encoding HA-KPNA2 **(A)**, HA-KPNA6 **(B)**, Flag-HDAC3, Myc-LRRK2-WT or Myc-LRRK2-KD alone or in combination. Total cell lysates were immunoprecipitated with anti-Flag antibody, followed by immunoblotting with anti-HA antibody. Expression of exogenous KPNA2 **(A)**, KPNA6 **(B)**, HDAC3, or LRRK2 in cell extracts was evaluated by immunoblotting with anti-HA, anti-Flag, or anti-Myc antibodies. **(C,D)** Where specified, HEK293 cells were transfected for 24 h with plasmids encoding HA-KPNA2 **(C)**, HA-KPNA6 **(D)**, Myc-LRRK2-WT or Myc-LRRK2-KD alone or in combination. Total cell lysates were immunoprecipitated with anti-phospho-Ser antibody, followed by immunoblotting with anti-HA antibody. Expression of exogenous KPNA2 **(C)**, KPNA6 **(D)**, or LRRK2 in cell extracts was evaluated by immunoblotting with anti-HA or anti-Myc antibodies (left panel). Data are representative of three independent experiments. Relative phosphorylated KPNA2/6 protein levels were quantified using the MultiGauge V. 3.1 program ($n = 3$; * $P < 0.05$; ** $P < 0.01$; right panel).

LRRK2 specifically promotes deacetylation of histone H4 with 6-OHDA treatment

Histones H2, H3 and H4 are reported to be substrates of HDAC3. H4, in particular, is thought to play a role in the initiation of HDAC3-mediated neuronal death (27). We examined whether knockout of *LRRK2* affects the acetylation level of histone H4. After nuclear fractions from *LRRK2* +/+ and *LRRK2* -/- MEFs were prepared, we compared the acetylation levels of H3, H4-K5 and H4-K12. Western blotting of cell lysates with antisera specific for each acetylated histone protein showed that *LRRK2* -/- MEFs had much greater inhibition of H4 deacetylation compared with *LRRK2* +/+ MEFs (Fig. 8A). Moreover, 6-OHDA treatment increased deacetylation of H4-K5 and H4-K12 by approximately 50% and 45%, respectively, in *LRRK2* +/+ MEFs; *LRRK2* -/- MEFs showed a slight reduction in acetylation at these sites (Fig. 8B). These results suggest that LRRK2 promotes the deacetylation of H4-K5 and H4-K12 with 6-OHDA treatment.

We next tested whether nuclear translocation of HDAC3 is also required for the deacetylation of histone H4 lysine residues. We transfected *LRRK2* -/- MEFs with Myc-tagged LRRK2-WT, Flag-HDAC3-WT, Flag-HDAC3-S424A, or/and Flag-HDAC3-S424E mutant, and compared the acetylation levels of H4-K5 and H4-K12 in the nuclear fractions. Our results showed that they were decreased in the presence of LRRK2-WT, and more reduced by co-expression of HDAC3-S424E with LRRK2-WT (Fig. 8C). However, this effect was not observed by co-expression of HDAC3-S424A mutant with LRRK2-WT (Fig. 8C). Moreover, all of these HDAC3 proteins had no significant effect on the levels of acetylated H4-K5 and H4-K12 in *LRRK2* -/- MEFs when transfected alone. Based on our previous finding that HDAC3-WT, HDAC3-S424A, or HDAC3-S424E mutant alone predominantly localized in the cytosol and co-expression of LRRK2-WT markedly stimulates their nuclear transport (Fig. 6A and B). These results suggest that LRRK2 promotes deacetylation of H4-K5 and H4-K12 residues through the phosphorylation and subsequent nuclear translocation of HDAC3.

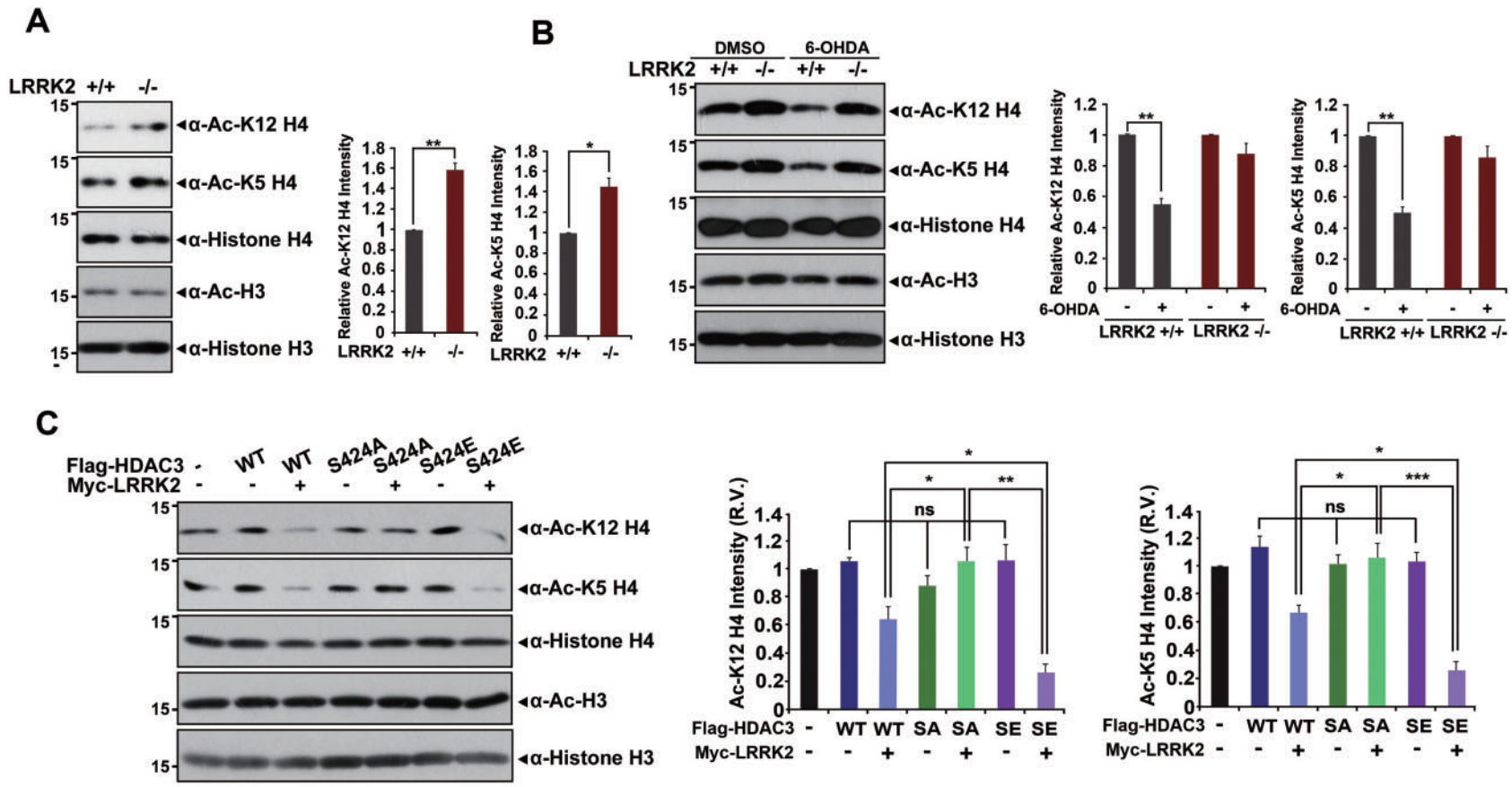

Figure 8. Acetylation of histone H4 is increased in *LRRK2* -/- MEFs. **(A)** Nuclear and cytoplasmic fractions from *LRRK2* +/+ and *LRRK2* -/- MEFs were prepared by cell fractionation. Nuclear fractions were subjected to western blotting using antisera specific for acetylated H4-K5, H4-K12, or acetylated H3 **(A-C)**. Endogenous H4 and H3 protein levels were analysed by immunoblotting with anti-H3 or anti-H4 antibodies (left panel) **(A-C)**. The graph on the right panel indicates the relative band intensities of acetylated H4-K5 or H4-K12 **(A-C)** quantified using Multi Gauge version 3.1. Data are expressed as the mean ± S.E.M of three independent experiments ($n = 3$; * $P < 0.05$, ** $P < 0.01$; *** $P < 0.001$, n.s., not significant). **(B)** *LRRK2* +/+ and *LRRK2* -/- MEFs were treated for 12 h with DMSO or 100 μM 6-OHDA and cell fractionation was performed. **(C)** Where specified, *LRRK2* -/- MEFs were transfected for 24 h with plasmids encoding Myc-tagged LRRK2-WT, Flag-tagged HDAC3-WT, HDAC-S424A, or HDAC-S424E alone or in combination. Nuclear fraction was prepared by cell fractionation.

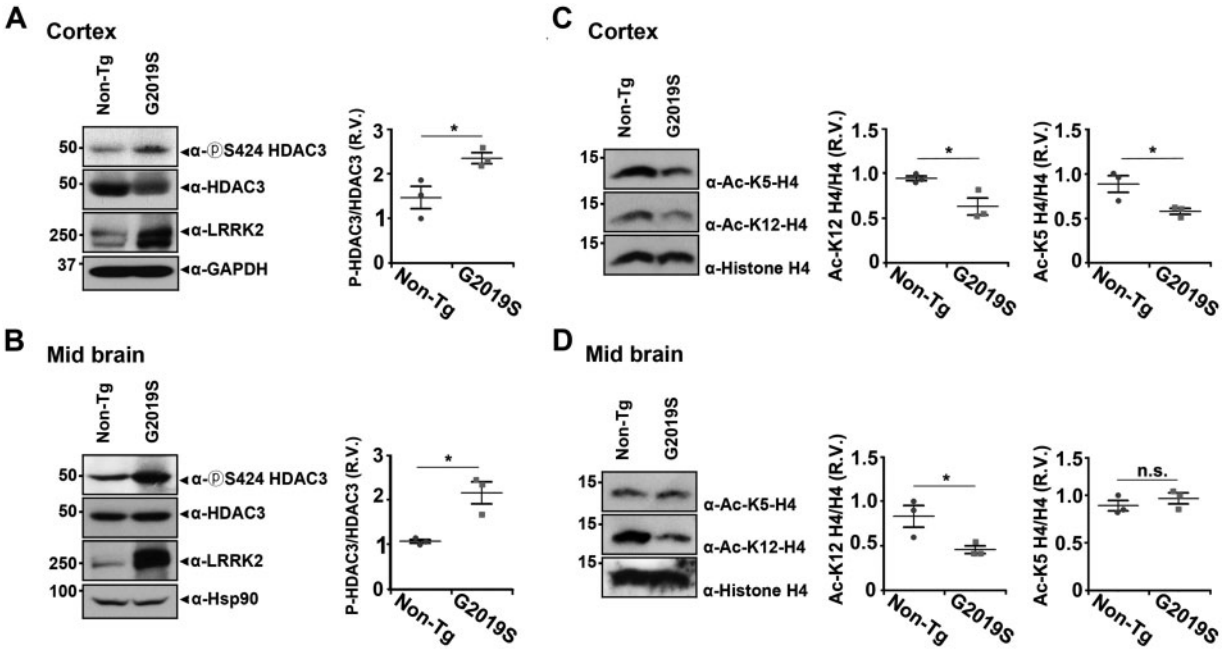

Figure 9. Increased phosphorylation of HDAC3 at Ser-424 and impaired acetylation of histone H4 are observed in aged LRRK2-G2019S Tg mice. **(A,B)** Brain lysates from the cortex **(A)** and mid-brain **(B)** regions of control and LRRK2-G2019S Tg mice were resolved using SDS-PAGE, and immunoblotted with anti-phospho-S424-HDAC3, anti-HDAC3, or anti-LRRK2 antibodies. To control for sample loading, immunoblotting with anti-Hsp90 or anti-GAPDH antibodies was also performed. **(C,D)** Brain lysates **(A, B)** were mixed with 1% SDS, separated by SDS-PAGE, and immunoblotted with anti-acetylated H4-K5 or anti-acetylated H4-K12 antibodies. Levels of endogenous histone H4 protein were detected and measured using an anti-histone H4 antibody. The graphs in A-D indicate the relative band intensities of phosphorylated HDAC3 **(A, B)** and acetylated H4-K5 or H4-K12 **(C, D)** quantified using MultiGauge version 3.1. Data are expressed as the mean ± S.E.M of three independent experiments ($n = 3$; * $P < 0.05$, n.s., not significant).

LRRK2 Tg mice show increased HDAC3 phosphorylation and greatly reduced histone H4 acetylation in the brain

We next investigated whether LRRK2 promotes the phosphorylation of HDAC3 and deacetylation of histone H4 lysine residues in the brains of 12-16 month-old Tg mice expressing LRRK2-G2019S (28). These BAC transgenic LRRK2-G2019S mice, displaying age-dependent decrease in striatal dopamine content as well as decreased striatal dopamine release and uptake, are widely utilized in investigations of the biological significance of LRRK2 overexpression in cultured cell lines. Furthermore, the brains of aged (12–16 months old) LRRK2 Tg mice may closely reflect those of PD patients, which also display significant neural degeneration (29). We first analysed gross changes in HDAC3 phosphorylation in the cortex and mid-brain regions of LRRK2-G2019S Tg mice. Western blotting of brain extracts showed that there were elevated levels of phosphorylated HDAC3-S424 in the cortex and mid-brain regions of LRRK2-G2019S Tg mice (Fig. 9A and B). Furthermore, when we examined the levels of acetylated H4-K5 and H4-K12, H4-K12 acetylation was greatly reduced in the cortex and mid-brain regions of LRRK2 Tg mice compared with controls. Deacetylation of H4-K5 was observed only in the cortex, but not the mid-brain region, of LRRK2-G2019S Tg mice (Fig. 9C and D). These results indicate that LRRK2 stimulates deacetylation of the H4-K12 residue, possibly through HDAC3 modification, which might play a role in LRRK2-induced neurodegeneration in the LRRK2 Tg mouse model.

LRRK2 inhibits transcriptional regulatory activity of MEF2D via phosphorylation of HDAC3-S424

MEF2D is a non-histone substrate of HDAC3. While HDAC3 can deacetylate MEF2D, other class I HDACs exhibit no obvious deacetylase activity towards MEF2D (17). Additionally, regulation of MEF2D activity is closely associated with neuronal survival. For example, MEF2D activation protects neuronal cells in the mouse substantia nigra pars compacta (30). Thus, we examined whether LRRK2 regulates MEF2D activity via HDAC3 phosphorylation. HEK293 cells were transfected with Flag-tagged HDAC3-WT alone or with Myc-tagged LRRK2-WT or LRRK2-KD. MEF2D reporter assays revealed that HDAC3 overexpression reduced MEF2D activity by approximately 20%, and co-expression of LRRK2-WT with HDAC3 further decreased MEF2D activity compared with cells transfected with HDAC3 alone (Supplementary Material, Fig. S3A). Transcriptional activity of MEF2D also decreased in cells transfected with LRRK2-WT alone, and this effect was rescued by treatment with trichostatin A (TSA), an HDAC class I and II inhibitor (Supplementary Material, Fig. S3B). Co-immunoprecipitation assays revealed that LRRK2 does not bind to MEF2D (Supplementary Material, Fig. S3D), suggesting that LRRK2 might regulate MEF2D activity through HDAC3 modulation. This hypothesis was supported by additional findings that overexpression of the phosphomimetic HDAC3-S424E mutant further suppressed MEF2D activity (Supplementary Material, Fig. S3C). In contrast, the phosphorylation-resistant HDAC3-S424A mutant markedly increased MEF2D activity (Supplementary Material, Fig. S3C). These data collectively suggest that LRRK2 negatively regulates MEF2D activity via phosphorylation of the HDAC3-S424 residue. As the proper MEF2D activity is closely associated with neuronal differentiation and cell survival (31,32), we then evaluated the effect of *MEF2D*-knockdown or its overexpression on SH-SY5Y cell viability. As expected, the cell viability was decreased by *MEF2D*-knockdown (Supplementary Material, Fig. S3E and F), whereas the overexpression of MEF2D correspondingly increased it (Supplementary Material, Fig. S3G).

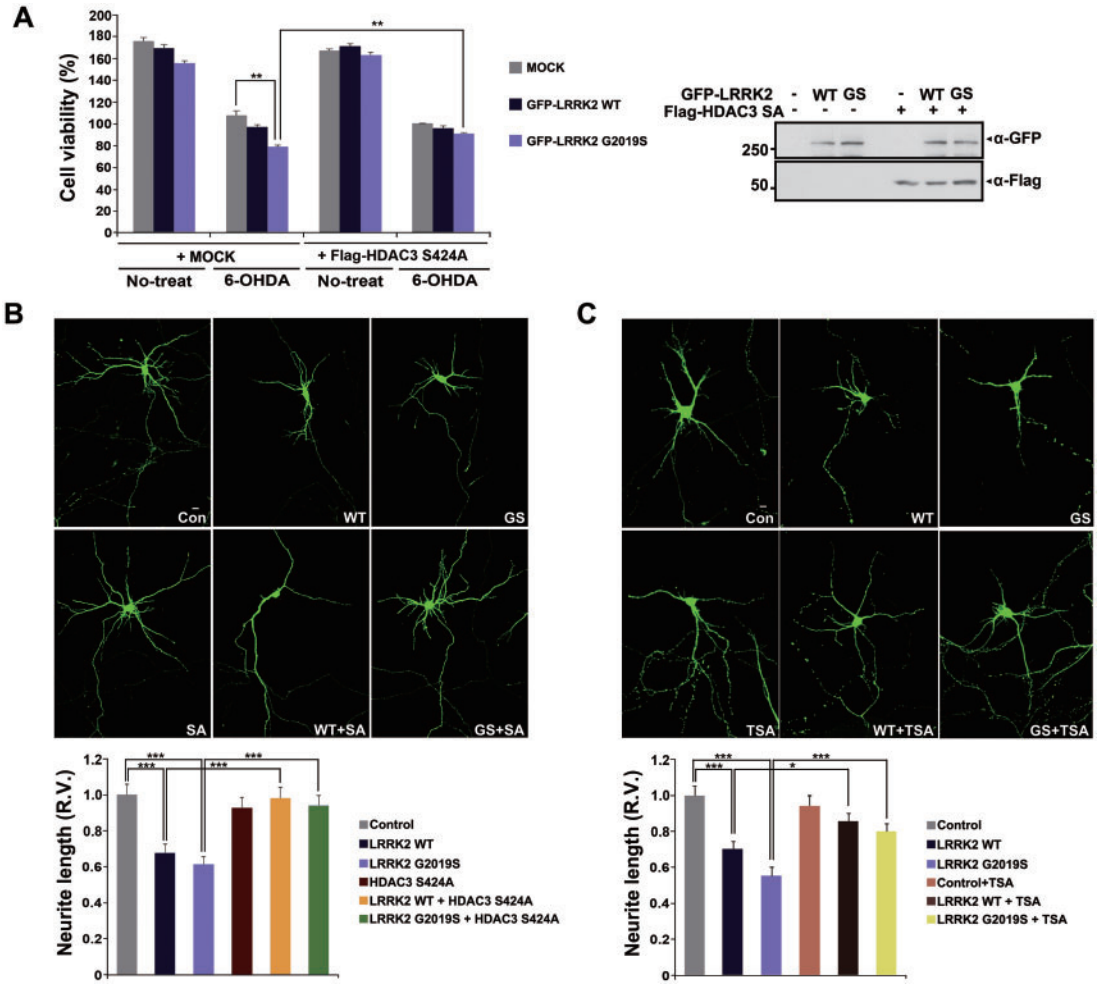

Figure 10. Overexpression of phosphorylation-resistant HDAC3 or treatment with HDAC inhibitor protects mammalian neuronal cells from LRRK2-induced cellular toxicity. **(A)** SH-SY5Y cells were mock-transfected or transfected for 36 h with plasmids encoding Flag-tagged HDAC3-S424A, GFP-tagged LRRK2-WT, or LRRK2-G2019S alone or in combination, as indicated. Cells were treated for an additional 12 h with DMSO or 100 μM 6-OHDA, and viability was assessed using a CCK-8 assay. Data are expressed as the mean ± S.E.M. of three independent experiments ($n = 9$; ** $P < 0.01$). **(B)** Where specified, rat primary cortical neurons were transfected for 3 days at DIV4 with plasmids encoding Myc-LRRK2-WT, Myc-LRRK2-G2019S, Flag-HDAC3-S424A, or GFP alone or in combination; images were obtained using confocal microscopy (LSM700; Carl Zeiss; upper panel). Neurite lengths of GFP-positive neurons were measured by MetaMorph software. Data are expressed as the mean ± S.E.M. (control, $n = 27$; WT, $n = 19$; GS, $n = 24$; SA, $n = 16$; WT+SA, $n = 13$; GS+SA, $n = 15$; *** $P < 0.001$; scale bars: 10 μm). **(C)** Where specified, rat primary cortical neurons at DIV4 were transfected for 3 days with GFP alone or together with Myc-LRRK2-WT or Myc-LRRK2-G2019S, and treated for 8 h with DMSO or TSA (3 μM). The images of each sample were obtained using confocal microscopy (LSM700; Carl Zeiss; upper panel). Neurite lengths of GFP-positive neurons were measured by MetaMorph software. Data are expressed as the mean ± S.E.M. (control, $n = 17$; WT, $n = 20$; GS, $n = 16$; control + TSA, $n = 22$; WT + TSA, $n = 20$; GS + TSA, $n = 19$; * $P < 0.05$; *** $P < 0.001$; scale bars: 10 μm).

Phosphorylation of HDAC3 potentiates LRRK2-G2019S cytotoxicity

The LRRK2-G2019S mutant has been previously shown to have a much greater neurotoxic effect than wild-type LRRK2 with 6-OHDA treatment (33). To determine whether HDAC3 can modulate the cytotoxic effects of LRRK2, we evaluated the effect of HDAC3-S424A on 6-OHDA-induced toxicity in SH-SY5Y cells. Cells were transfected with GFP-tagged LRRK2-WT or LRRK2-G2019S mutant alone or with Flag-HDAC3-S424A, and treated with dimethyl sulfoxide (DMSO) or 6-OHDA. Treatment with 6-OHDA triggered significant cell death in cells expressing the LRRK2-G2019S mutant, reducing cell viability by approximately 40% (Fig. 10A). In contrast, transfection with LRRK2-G2019S and HDAC3-S424A restored cell viability to control levels with 6-OHDA treatment. These data suggest that HDAC3 phosphorylation is important in mediating the cytotoxic effects of LRRK2 in response to treatment with 6-OHDA.

Based on previous findings that LRRK2 negatively regulates the length and complexity of neuronal processes in primary neurons (34–36), we investigated the effects of phosphorylated HDAC3 on LRRK2-induced neurite retraction. Rat primary cortical neurons were transfected with GFP alone or with either Myc-tagged LRRK2-WT, LRRK2-G2019S, or Flag-tagged HDAC3-S424A, and neurite lengths were quantified. LRRK2-WT alone caused significant retraction of neurite outgrowth; LRRK2-G2019S also significantly reduced neurite length to a similar extent (Fig. 10B). Co-expression of HDAC3-S424A attenuated this inhibitory effect, whereas the HDAC3-S424A mutant alone had no significant effect on cell viability (Fig. 10B). Moreover, the neurite retraction induced by LRRK2 was rescued back by the

treatment of trichostatin A (TSA), an HDAC class I and II inhibitor (Fig. 10C). Collectively, these data suggest that HDAC3 mediates LRRK2-induced toxicity.

Discussion

The kinase LRRK2 phosphorylates a diverse array of substrates, affecting their function and various signalling pathways. Firstly, LRRK2 phosphorylates many vesicle trafficking-related proteins. For example, it phosphorylates Rab5B at its Thr-6 residue and increases its GTPase activity, which then inhibits endocytosis of synaptic vesicles (37). Secondly, LRRK2 targets transcription factors and modulates their transcriptional activities. For example, LRRK2 phosphorylates the Ser-319 residue of FoxO1, increasing its transcriptional activity (38). In addition, several neurodegenerative disease-related proteins are the substrates of LRRK2, including α-synuclein in PD (39) and tau in Alzheimer's disease (40). Lastly, LRRK2 participates in a number of signalling pathways. For instance, LRRK2 phosphorylates the Ser-473 residue of Akt (41). LRRK2 also phosphorylates many types of mitogen-activated protein kinase (MKK), such as MKK3, 4, 6 and 7 (42,43). Here, we identify HDAC3 as a novel substrate of LRRK2. This relationship influences the epigenetic regulation through modulation of histone conformation.

Our *in vitro* kinase assays revealed that LRRK2 phosphorylates HDAC3 at its Ser-424 residue. In addition to LRRK2, multiple kinases phosphorylate HDAC3. For example, c-Src, GSK-3β, CK2 and PINK1 phosphorylate HDAC3 and regulate its enzymatic and/or cytotoxic activities (12,20,23,25). With regard to HDAC3, its Ser-424 residue is the only reported target for phosphorylation that is important for its deacetylase activity. For example, CK2 (23) and PINK1 (20) phosphorylate HDAC3 at Ser-424 and stimulate HDAC3 deacetylase activity. PINK1, like LRRK2, is one of many genetic factors suspected of causing the familial form of PD. Interestingly, PINK1-mediated HDAC3-S424 phosphorylation blocks caspase-dependent cleavage of HDAC3 in response to treatment with hydrogen peroxide (20). Consistent with these findings, cleavage of the phosphorylation-resistant HDAC3-S424A mutant was not affected by PINK1. This same phenomenon has also been observed with the HDAC3-Y298F mutant, which lacks deacetylase activity, even though its Ser-424 residue can be still phosphorylated. These findings suggest that PINK1 mainly controls HDAC3 activity by blocking its degradation. Therefore, preventing cleavage of HDAC3 may be a unique function of PINK1. Unlike these two kinases, LRRK2 affects not only HDAC3 activity, but also its intracellular localization. Nuclear translocation of HDAC3 is mediated by LRRK2, which occurs not through phosphorylation of HDAC3, but rather through an increase in HDAC3 binding to KPNA-2/6. As a consequence, accumulation of HDAC3 in the nucleus stimulates lysine modification at target histones.

The shuttling and redistribution process between the cytoplasm and nucleus is important for the proper function of HDAC3. Previous study demonstrated that HDAC3 displays differential effect on the cytoplasmic and nuclear huntingtin aggregates (44). Likewise, the precise nuclear transport of HDAC3 would be a key factor for its primary role of histone modification and chromosome dynamics, though the detailed mechanism is not clearly defined. In the present study, we firstly identified that KPNA2 and 6 are the novel substrates of LRRK2 and play a role in the shuttling of HDAC3, possibly through phosphorylation.

Many studies have demonstrated that LRRK2 directly affects gene transcription. For example, RNA interference-induced depletion of LRRK2 alters the expression of approximately 200 genes by a factor of at least 1.5 in SH-SY5Y cells and LRRK2 +/- embryonic stem cells, whereas changes in genetic expression were identified using microarrays (45,46). Additionally, LRRK2 affects the activities of some transcription factors. For example, LRRK2 negatively regulates the nuclear factor of activated T cells (NFAT) (47), and LRRK2 overexpression increases the transcriptional activity of NF-κB (48). In contrast, LRRK2 knockdown blocks NF-κB activity upon the stimulation with LPS (49). Despite numerous investigations, the molecular mechanism underlying LRRK2-mediated regulation of gene transcription remains poorly understood. Here, we provide evidence that LRRK2 negatively regulates MEF2D-mediated gene transcription through phosphorylation of HDAC3. Moreover, the present work demonstrates that LRRK2 modulates gene transcription indirectly through phosphorylation of HDAC3, histone deacetylation and histone-mediated epigenetic control.

HDAC3 has many nuclear substrates, including histones. Among them, histones H3 and H4 mediate nuclear condensation, causing cell death by modifying the acetylation state of lysine residues (50). Based on these findings, we investigated the effects of LRRK2-mediated HDAC3 phosphorylation on H3 and H4 acetylation state. Analysis of nuclear samples from *LRRK2* -/- and *LRRK2* +/+ MEFs showed that there was enhanced deacetylation of H4-K5 and H4-K12 in *LRRK2* +/+ MEFs. In contrast, acetylation of H3 at several lysine residues was not significantly affected. These results indicate that LRRK2 specifically stimulates deacetylation at H4-K5 and H4-K12 by phosphorylating and activating HDAC3. Subsequent to histone deacetylation, downstream effects leading to neuronal cell death may involve neurite shortening, which was observed in model systems overexpressing wild-type LRRK2 or a LRRK2 mutation. This hypothesis was corroborated by findings that LRRK2-mediated HDAC3 phosphorylation exacerbated neurite shortening in primary cortical neurons, which could be an underlying mechanism of neuronal cell death.

PD-associated LRRK2 mutants can trigger toxicity in neuronal cells, wherein the enhanced kinase activity is critical to this process, and the underlying mechanisms are largely unknown. For example, the G2019S mutation in *LRRK2* has been shown to increase the sensitivity of human dopaminergic neurons to 6-OHDA (33). We also found that 6-OHDA markedly enhanced LRRK2 kinase activity, which increased the phosphorylation and nuclear translocation of HDAC3 in SH-SY5Y cells. Furthermore, 6-OHDA treatment selectively facilitates deacetylation of H4-K5 and H4-K12 residues, which then exacerbates neuronal cell death. Interestingly, levels of acetylated H4-K5 and H4-K12 were reduced in the brains of aged LRRK2-G2019S Tg mice, while they were elevated in *LRRK2* -/- MEFs. We did not observe alterations in the acetylation of H4-K5 in the mid-brain regions of aged *LRRK2-G2019S* Tg mice. While this aspect of our results remains to be explored, these data suggest that the acetylation state of H4-K12 might be an important factor in neuronal cell death in mid-brain regions, including the substantia nigra.

Evidence suggest that LRRK2-induced toxicity involves alterations in cytoskeletal dynamics, autophagy, mitochondrial dysfunction and extrinsic cell death pathways. For example, LRRK2-R1441G BAC Tg mice show enhanced phosphorylation of tau, which is associated with disruption of the microtubule network. This phosphorylation also likely plays a role in the retraction of neurites in cellular and *in vivo* models of LRRK2 mutants (51). Additionally, overexpression of the LRRK2-G2019S mutant causes accumulation of autophagic vacuoles; additionally,

up-regulation of inducers of autophagy potentiates the neurite shortening triggered by this mutant (52). Regarding a potential link between LRRK2 and extrinsic cell death pathways, LRRK2 is known to bind the Fas-associated protein with death domain (FADD), and PD-associated mutations enhance this interaction, which plays an important role in LRRK2-induced and caspase 8-dependent neuronal death (53). Here, we further demonstrate that the neurotoxic effects of LRRK2 may be additionally mediated by its phosphorylation of HDAC3 and downstream modulation of histone conformation and MEF2D activity.

To conclude, our results strongly suggest that HDAC3 phosphorylation by LRRK2 plays a role in LRRK2-mediated neuronal cell death and PD pathogenesis.

Materials and Methods

Materials

Peroxidase-conjugated anti-rabbit and anti-mouse antibodies were purchased from Millipore. (Billerica, MA, USA). Dulbecco's modified Eagle's medium (DMEM), fetal bovine serum (FBS) and lipofectamine and PLUS reagents were purchased from Life Technologies (Grand Island, NY, USA). 6-Hydroxydopamine (6-OHDA) hydrobromide, phospho-Ser-specific antibody and the anti-Flag antibody were purchased from Sigma-Aldrich (St. Louis, MO, USA). Mouse monoclonal anti-HDAC3 and rabbit polyclonal anti-phospho-HDAC3 (S424) antibodies were purchased from Millipore (Billerica, MA, USA) and Cell Signaling Technology (Danvers, MA, USA), respectively. Anti-Myc, anti-GAPDH and polyclonal anti-HDAC3 antibodies were purchased from Santa Cruz Biotechnology (Santa Cruz, CA, USA). Anti-LRRK2, anti-H3 and anti-acetylated H4-K12 antibodies were purchased from Abcam (Cambridge, MA, USA). Anti-eGFP antibody was purchased from Rockland (Gilbertsville, PA, USA). Polyclonal and monoclonal anti-HA IgGs were purchased from Abnova (Tebu, France) and Covance (Powhatan, VA, USA). Anti-H4, anti-acetylated H4-K5 and anti-acetylated H3 antiserum were purchased from Millipore. Protein A-sepharose and glutathione-sepharose 4B beads were purchased from GE Healthcare Life Science (Piscataway, NJ, USA). Enhanced chemiluminescence (ECL) reagent and [γ-^{32}P] ATP were purchased from PerkinElmer Life and Analytical Sciences (Waltham, MA, USA). All other chemicals and reagents were analytical grade commercial products and purchased from Sigma-Aldrich.

DNA constructs

Mammalian constructs encoding Myc-tagged wild-type LRRK2 (LRRK2-WT), its kinase-dead mutant with a point mutation at D1994A (LRRK2-KD), or two PD-linked point mutants at G2019S (LRRK2-G2019S) or R1441C (LRRK2-R1441C) were generated, as described previously (54,55). The plasmids pDEST53-LRRK2-WT and pDEST53-LRRK2-G2019S with an N-terminal-GFP-tag were purchased from Addgene (Cambridge, MA, USA). The plasmid encoding Flag-tagged HDAC3 was provided by E. Seto (H. Lee Moffitt Cancer Center and Research Institute, Tampa, FL, USA). The myocyte-specific enhancer factor 2D (MEF2D)-driven reporter plasmid was kindly provided by H.D. Youn (Seoul National University, Seoul, Republic of Korea). Plasmids encoding HA-tagged KPNA1, 2, 3, 4 and 6 were kindly provided by I.K. Chung (Yonsei University, Seoul, Korea). Bacterial constructs encoding GST-fused wild-type HDAC3 (pGEX4T-1-GST-HDAC3) and its deletion mutants were constructed through PCR amplification and sub-cloning into a pGEX4T-1 vector. Several bacterial constructs encoding GST-fused HDAC3 with single, double, or triple point mutations in the nuclear localization signal (NLS) domain were produced through PCR amplification using pGEX4T-1-GST-HDAC3 as a template, and the corresponding site-directed mutagenesis reactions were performed using the QuikChange TM Site-Directed Mutagenesis Kit (Agilent Technologies, Santa Clara, CA USA) according to the manufacturer's instructions.

Cell cultures and DNA transfection

Human embryonic kidney 293 (HEK293) cells, human neuroblastoma SH-SY5Y cells and mouse embryonic fibroblasts (MEFs) derived from wild-type or *LRRK2*-knockout mice were maintained in DMEM containing 10% FBS and 100 units/ml penicillin-streptomycin. Rat cortical neuron cultures were prepared from embryonic day 18 (E18) embryos. Cortical neurons were dissected and plated on coverslips coated with poly-D-lysine. Cells were grown in neurobasal media supplemented with 2% B-27 (Invitrogen, Grand Island, NY, USA), 0.5% FBS, 0.5 mM Glutamax (Invitrogen), 1 mM sodium pyruvate and 100 units/ml penicillin-streptomycin. After 3-4 days *in vitro* (DIV), DNA transfections were performed using Lipofectamine 2000 (Invitrogen) according to the manufacturer's instructions.

RNA interference

Small interfering RNAs (siRNA) targeting *LRRK2* was purchased from Invitrogen (Cat No. 272780). The *MEF2D*-specific and scrambled control siRNAs were purchased from Bioneer (Seoul, Korea). For these experiments, neuroblastoma SH-SY5Y cells were transfected with siRNAs for 48 h using Lipofectamine 2000.

Preparation of cell lysates

Cells were rinsed with ice-cold phosphate-buffered saline (PBS) and solubilized using lysis buffer containing 10 mM Tris (pH 7.4), 1% Nonidet P-40 (NP-40), 150 mM NaCl, 10% glycerol, 1 mM Na_3VO_4, 1 μg/ml leupeptin, 1 μg/ml aprotinin, 10 mM NaF and 0.2 mM phenylmethylsulfonyl fluoride (PMSF), and then briefly sonicated. Lysates were clarified by centrifugation at 13,000 x g for 20 min at 4 °C.

Immunoprecipitation and western blots

One μg of the appropriate antibody was incubated overnight at 4 °C with 800 μg of cell extracts prepared in lysis buffer. The mixture was subsequently incubated with gentle rotation for 2 h at 4 °C with 30 μl of a 1:1 suspension of protein A-sepharose beads. The beads were pelleted and washed three times with lysis buffer. Immunocomplexes were dissociated by boiling the mixture in 2X SDS-PAGE sample buffer. Whole protein samples were separated by SDS-PAGE and transferred to a nitrocellulose membrane. The membrane was blocked with Tris-buffered saline with Tween 20 (TBST) buffer containing 20 mM Tris (pH 7.5), 137 mM NaCl, 0.1% Tween® 20 and 5% non-fat dry milk for 1 h at room temperature, and then incubated overnight at 4 °C in 3% non-fat dry milk containing the appropriate primary antibodies. The membrane was washed several times in TBST and incubated for 2 h with horseradish peroxidase (HRP)-coupled secondary IgG. The membrane was washed several times with TBST and bands were visualized using ECL reagents.

Phos-tag immunoblotting

After the DNA transfection for 24 h, cells were rinsed in ice-cold PBS and lysed on ice with lysis buffer containing 0.2% NP-40, 50 mM Tris (pH 7.4), 150 mM NaCl, 10% glycerol, 0.2 mM PMSF, 1 μg/ml aprotinin, 1 μg/ml leupeptin, 1 mM Na_3VO_4 and 10 mM NaF. Phospho-HDAC3 was separated on 10% SDS-PAGE gel containing 30 mM phos-tag (Wako Pure Chemical Industries, Ltd., Japan). Phos-tag immunoblotting was performed according to the manufacturer's instructions.

Immunocytochemistry

HEK293, SH-SY5Y cells and rat cortical neurons were washed with PBS and fixed with 3.7% formaldehyde in PBS containing 4% sucrose for 10 min. After fixation, cells were washed twice with PBS and permeabilized with 0.2% Triton-X-100 for 10 min. Cells were blocked with a mixture of 3% horse serum and 0.1% bovine serum albumin in PBS for 30 min and incubated with an appropriate dilution of primary antibody. After washing twice with PBS, cells were incubated with Alexa Fluor 488, Alexa Fluor 594 (both from Invitrogen), Cy3, or fluorescein isothiocyanate (FITC)-conjugated secondary antibodies (both from Jackson ImmunoResearch, West Grove, PA, USA). Cells were then subjected to additional washes with PBS. Immunostained cells were observed using a Carl Zeiss LSM700 META confocal microscope. Primary cortical neurons were randomly chosen and images acquired using a 10x objective lens; all image settings were kept constant. Z-stack images obtained by confocal microscopy were converted into maximal projections.

Purification of bacterial recombinant HDAC3 protein

E. coli BL21 bacteria were transformed with pGEX4T-1-GST-HDAC3, and the expression of GST-HDAC3 was induced with the addition of 0.05 mM isopropyl β-D-1-thiogalactopyranoside for 3 h at 30 °C. Cells were sonicated while in PBS and centrifuged at 15,000 × *g* for 30 min at 4 °C. The resulting supernatant was incubated with glutathione-sepharose 4B overnight at 4 °C with gentle rotation. The beads were pelleted by centrifugation at 6,000 × *g* for 30 sec at 4 °C and washed three times with PBS. To exclude the potential confounding effects of GST, recombinant proteins were eluted with elution buffer (50 mM Tris, pH 8.0 and 25 mM reduced glutathione).

GST pull-down assays

GST pull-down assays were performed by incubating lysates with GST or GST-fused HDAC3 immobilized onto sepharose beads for 2 h or overnight at 4 °C. The mixtures were then washed three times with wash buffer [25 mM Tris-HCl (pH 7.5), 1 mM dithiothreitol (DTT), 30 mM $MgCl_2$, 40 mM NaCl and 1% NP-40]. Bound proteins were eluted with 2X SDS buffer, separated by SDS-PAGE, and subjected to Western blot analysis.

In vitro kinase assays

Cells were lysed with 1% NP-40 lysis buffer and cell lysates were immunoprecipitated with anti-Myc antibody overnight at 4 °C. Anti-Myc immunocomplexes were incubated with 30 μl of a 1:1 protein A-sepharose bead suspension for 2 h at 4 °C with gentle inversion. Beads were centrifuged at 6,000 × *g* for 30 sec, washed twice with lysis buffer, and then washed twice with 1X kinase reaction buffer [20 mM HEPES (pH 7.4), 15 mM $MgCl_2$, 5 mM EGTA, 0.1% Triton X-100, 0.5 mM DTT and 1 mM glycerophosphate]. Anti-LRRK2 immunocomplexes were mixed with 2 μg of bacterial recombinant wild-type HDAC3 fused to GST or its various deletion or point mutants, and then mixed with 1X kinase reaction buffer containing 10 μM cold ATP. The *in vitro* kinase reaction was initiated by the addition of 5 μCi [γ-^{32}P] ATP. The reaction was allowed to proceed for 15 min at 30 °C and was terminated by the addition of SDS-PAGE sample buffer. Protein samples were resolved by SDS-PAGE and incorporated [γ-^{32}P] radioisotope was detected using autoradiography.

HDAC assays

To perform HDAC assays on HEK293 cells, an HDAC-Glo™ I/II kit (Promega, Madison, WI, USA) was used according to the manufacturer's instructions. Briefly, HDAC3 immunocomplexes and HDAC-Glo™ I/II buffer (50 μl total) were incubated at room temperature for 60 sec using an orbital shaker to ensure homogeneity. A 50-μl mixture of HDAC-Glo™ I/II substrate and the developer reagent was added to the samples, which were mixed using an orbital shaker at room temperature for 1 min. Luminescence was measured using a Victor X3 multi-label plate reader (PerkinElmer).

Preparation of cytosolic and nuclear fractions

Cells were scrapped with ice-cold PBS and re-suspended in hypotonic buffer [10 mM HEPES (pH 7.9), 1.5 mM $MgCl_2$, 10 mM KCl, 0.5 mM DTT, 0.2 mM PMSF, 1 μg/ml aprotinin, 1 μg/ml leupeptin, 1 mM Na_3VO_4 and 10 mM NaF]. The cells were incubated for 10 min on ice and 0.5% NP-40 was added, followed by brief vortexing. Cell lysates were centrifuged at 15,000 × *g* for 5 min at 4 °C. The supernatants were used as the cytosolic fractions. Nuclear pellets were washed with hypotonic buffer and re-suspended with hypertonic buffer [27 mM HEPES (pH 7.9), 2 mM $MgCl_2$, 560 mM NaCl, 270 mM EDTA, 33% glycerol, 0.5 M DTT, 0.2 mM PMSF, 1 μg/ml aprotinin, 1 μg/ml leupeptin, 1 mM Na_3VO_4 and 10 mM NaF). The pellets were lysed with 1% NP-40, vortexed for 10 sec several times, incubated for 20 min on ice, and then were centrifuged at 15,000 × *g* for 20 min at 4 °C. These supernatants were used as the nuclear fractions.

Animal care

LRRK2 transgenic (Tg) mice expressing the G2019S mutant [FVB/N-Tg (LRRK2*G2019S) 1Cjli/J] were purchased from Jackson Laboratory (Bar Harbor, ME, USA) and maintained on a 12-h light/dark cycle. Mice were given *ad libitum* access to food and water. Female mice 12–18 months old with obvious behavioural symptoms and littermate controls were used for this study. All experimental procedures utilizing this *in vivo* PD model system followed guidelines approved by the Institutional Animal Care and Use Committee of Hanyang University (HY-IACUC-11-018 and HY-IACUC-12-018).

Preparation of LRRK2 Tg mouse brain tissues

Brains were dissected to acquire protein samples from the frontal cortex (FC) and mid-brain (MB). Protein samples were prepared in homogenization buffer (1% NP-40 lysis buffer, 1 mM EDTA and 0.1% or 1% SDS). The lysates were centrifuged for 30 min at 15,000 × *g* at 4°C and the supernatant was collected for experiments.

MEF2D-specific luciferase reporter assay

After a 24-h transfection period with a MEF2D-dependent firefly luciferase reporter and the Renilla luciferase plasmid, HEK293 cells were harvested in a passive lysis buffer (Promega, Madison, WI, USA), and luciferase assays were performed using the Dual-Luciferase Reporter Assay System (Promega). Relative luciferase activity was calculated by dividing the firefly luciferase activity by Renilla luciferase activity. The data represent three independent experiments performed in triplicate.

Cell viability assay

SH-SY5Y cells were transfected for 36 h with plasmids encoding GFP-tagged LRRK2-WT or the G2019S mutant alone or with Flag-HDAC3-S424A. Cells were treated for an additional 12 h with DMSO or 100 μM 6-OHDA. After removal of the media, Cell Counting Kit-8 (CCK-8, Dojindo Laboratories, Kumamoto, Japan) solution was added to each well. The plate was incubated for 30 min at 37 °C and absorbance was measured at 450 nm using a microplate reader.

Quantification of neurite length

Rat cortical neurons at DIV4 were transfected with GFP alone or with plasmids encoding Myc-LRRK2 and/or Flag-HDAC3-S424A and immunostained with antibodies against GFP at DIV8. Fluorescent images were acquired using a confocal microscope and neurite length measurements were performed using MetaMorph Software (Molecular Devices, Sunnyvale, CA, USA). All analyses were performed by a blinded investigator.

Statistical analysis

Group means were compared using Student's *t*-tests. *P* values ≤ 0.05 were considered statistically significant. Values are reported as the mean ± standard error of the mean (SEM).

Supplementary Material

Supplementary Material is available at *HMG* online.

Acknowledgements

The authors thank to E. Seto, I.K. Chung and H.D. Youn for providing the plasmids and to J.W. Um for the technical assistance.

Conflict of Interest statement. None declared.

Funding

This work was supported by grants from the Korea Healthcare Technology R&D Project through the Korea Health Industry Development Institute (KHIDI) funded by the Ministry of Health & Welfare (HI14C0093 to K.C.C.), and from the National Research Foundation of Korea (NRF) funded by the Ministry of Science, ICT & Future Planning (2014M3C7A1064545 to K.C.C.), Republic of Korea. This work was also supported in part by the NRF grant (2015R1A2A2A01003080 to K.C.C.) and by Yonsei University Future-leading Research Initiative of 2015 (2015-22-0055 to K.C.C.).

References

1. Olanow, C.W. and Tatton, W.G. (1999) Etiology and pathogenesis of Parkinson's disease. *Annu. Rev. Neurosci.*, **22**, 123–144.
2. Moore, D.J., West, A.B., Dawson, V.L. and Dawson, T.M. (2005) Molecular pathophysiology of Parkinson's disease. *Annu. Rev. Neurosci.*, **28**, 57–87.
3. Seol, W. (2010) Biochemical and molecular features of LRRK2 and its pathophysiological roles in Parkinson's disease. *BMB Rep.*, **43**, 233–244.
4. Cookson, M.R. (2010) The role of leucine-rich repeat kinase 2 (LRRK2) in Parkinson's disease. *Nat. Rev. Neurosci.*, **11**, 791–797.
5. Smith, W.W., Pei, Z., Jiang, H., Dawson, V.L., Dawson, T.M. and Ross, C.A. (2006b) Kinase activity of mutant LRRK2 mediates neuronal toxicity. *Nat. Neurosci.*, **9**, 1231–1233.
6. West, A.B., Moore, D.J., Choi, C., Andrabi, S.A., Li, X., Dikeman, D., Biskup, S., Zhang, Z., Lim, K.L., Dawson, V.L.,. and Dawson, T.M. (2007) Parkinson's disease-associated mutations in LRRK2 link enhanced GTP-binding and kinase activities to neuronal toxicity. *Hum. Mol. Genet.*, **16**, 223–232.
7. Jaleel, M., Nichols, R.J., Deak, M., Campbell, D.G., Gillardon, F., Knebel, A. and Alessi, D.R. (2007) LRRK2 phosphorylates moesin at threonine-558: characterization of how Parkinson's disease mutants affect kinase activity. *Biochem. J.*, **405**, 307–317.
8. Esteves, A.R., Swerdlow, R.H. and Cardoso, S.M. (2014) LRRK2, a puzzling protein: Insights into Parkinson's disease pathogenesis. *Exp. Neurol.*, **261**, 206–216.
9. Yang, W.M., Yao, Y.L., Sun, J.M., Davie, J.R. and Seto, E. (1997) Isolation and characterization of cDNAs corresponding to an additional member of the human histone deacetylase gene family. *J. Biol. Chem.*, **272**, 28001–28007.
10. de Ruijter, A.J., van Gennip, A.H., Caron, H.N., Kemp, S. and van Kuilenburg, A.B. (2003) Histone deacetylases (HDACs): characterization of the classical HDAC family. *Biochem. J.*, **370**, 737–749.
11. Yang, W.M., Tsai, S.C., Wen, Y.D., Fejer, G. and Seto, E. (2002) Functional domains of histone deacetylase-3. *J. Biol. Chem.*, **277**, 9447–9454.
12. Longworth, M.S. and Laimins, L.A. (2006) Histone deacetylase 3 localizes to the plasma membrane and is a substrate of Src. *Oncogene.*, **25**, 4495–4500.
13. Johnson, C.A., White, D.A., Lavender, J.S., O'Neill, L.P. and Turner, B.M. (2002) Human class I histone deacetylase complexes show enhanced catalytic activity in the presence of ATP and co-immunoprecipitate with the ATP-dependent chaperone protein Hsp70. *J. Biol. Chem.*, **277**, 9590–9597.
14. Hartman, H.B., Yu, J., Alenghat, T., Ishizuka, T. and Lazar, M.A. (2005) The histone-binding code of nuclear receptor corepressors matches the substrate specificity of histone deacetylase 3. *EMBO Rep.*, **6**, 445–451.
15. Bhaskara, S., Knutson, S.K., Jiang, G., Chandrasekharan, M.B., Wilson, A.J., Zheng, S., Yenamandra, A., Locke, K., Yuan, J.L., Bonine-Summers, A.R., *et al.* (2010) Hdac3 is essential for the maintenance of chromatin structure and genome stability. *Cancer Cell*, **18**, 436–447.
16. Knutson, S.K., Chyla, B.J., Amann, J.M., Bhaskara, S., Huppert, S.S. and Hiebert, S.W. (2008) Liver-specific deletion of histone deacetylase 3 disrupts metabolic transcriptional networks. *Embo J.*, **27**, 1017–1028.
17. Grégoire, S., Xiao, L., Nie, J., Zhang, X., Xu, M., Li, J., Wong, J., Seto, E. and Yang, X.J. (2007) Histone deacetylase 3 interacts with and deacetylates myocyte enhancer factor 2. *Mol. Cell. Biol.*, **27**, 1280–1295.

18. Chen, L., Fischle, W., Verdin, E. and Greene, W.C. (2001) Duration of nuclear NF-kappaB action regulated by reversible acetylation. *Science*, **293**, 1653–1657.
19. Nicolas, E., Ait-Si-Ali, S. and Trouche, D. (2001) The histone deacetylase HDAC3 targets RbAp48 to the retinoblastoma protein. *Nucleic Acids Res.*, **29**, 3131–3136.
20. Choi, H.K., Choi, Y., Kang, H., Lim, E.J., Park, S.Y., Lee, H.S., Park, J.M., Moon, J., Kim, Y.J., Choi, I., *et al.* (2015) PINK1 positively regulates HDAC3 to suppress dopaminergic neuronal cell death. *Hum. Mol. Genet.*, **24**, 1127–1141.
21. Bates, E.A., Victor, M., Jones, A.K., Shi, Y. and Hart, A.C. (2006) Differential contributions of Caenorhabditis elegans histone deacetylases to huntingtin polyglutamine toxicity. *J. Neurosci.*, **26**, 2830–2838.
22. Bardai, F.H., Price, V., Zaayman, M., Wang, L. and D'Mello, S.R. (2012) Histone deacetylase-1 (HDAC1) is a molecular switch between neuronal survival and death. *J. Biol. Chem.*, **287**, 35444–35453.
23. Zhang, X., Ozawa, Y., Lee, H., Wen, Y.D., Tan, T.H., Wadzinski, B.E. and Seto, E. (2005) Histone deacetylase 3 (HDAC3) activity is regulated by interaction with protein serine/threonine phosphatase 4. *Genes Dev.*, **19**, 827–839.
24. Jeyakumar, M., Liu, X.F., Erdjument-Bromage, H., Tempst, P. and Bagchi, M.K. (2007) Phosphorylation of thyroid hormone receptor-associated nuclear receptor corepressor holocomplex by the DNA-dependent protein kinase enhances its histone deacetylase activity. *J. Biol. Chem.*, **282**, 9312–9322.
25. Bardai, F.H. and D'Mello, S.R. (2011) Selective toxicity by HDAC3 in neurons: regulation by Akt and GSK3beta. *J. Neurosci.*, **31**, 1746–1751.
26. Guenther, M.G., Barak, O. and Lazar, M.A. (2001) The SMRT and N-CoR corepressors are activating cofactors for histone deacetylase 3. *Mol. Cell. Biol.*, **21**, 6091–6101.
27. Pelzel, H.R., Schlamp, C.L. and Nickells, R.W. (2010) Histone **H4** deacetylation plays a critical role in early gene silencing during neuronal apoptosis. *BMC Neurosci.*, **11**, 62.
28. Li, X., Patel, J.C., Wang, J., Avshalumov, M.V., Nicholson, C., Buxbaum, J.D., Elder, G.A., Rice, M.E. and Yue, Z. (2010) Enhanced striatal dopamine transmission and motor performance with LRRK2 overexpression in mice is eliminated by familial Parkinson's disease mutation G2019S. *J. Neurosci.*, **30**, 1788–1797.
29. Chen, C.Y., Weng, Y.H., Chien, K.Y., Lin, K.J., Yeh, T.H., Cheng, Y.P., Lu, C.S. and Wang, H.L. (2012) (G2019S) LRRK2 activates MKK4-JNK pathway and causes degeneration of SN dopaminergic neurons in a transgenic mouse model of PD. *Cell Death Differ.*, **19**, 1623–1633.
30. Smith, P.D., Mount, M.P., Shree, R., Callaghan, S., Slack, R.S., Anisman, H., Vincent, I., Wang, X., Mao, Z. and Park, D.S. (2006a) Calpain-regulated p35/cdk5 plays a central role in dopaminergic neuron death through modulation of the transcription factor myocyte enhancer factor 2. *J. Neurosci.*, **26**, 440–447.
31. Wang, B., Cai, Z., Lu, F., Li, C., Zhu, X., Su, L., Gao, G. and Yang, Q. (2014) Destabilization of survival factor MEF2D mRNA by neurotoxin in models of Parkinson's disease. *J. Neurochem.*, **130**, 720–728.
32. Lam, B.Y. and Chawla, S. (2007) MEF2D expression increases during neuronal differentiation of neural progenitor cells and correlates with neurite length. *Neurosci. Lett.*, **427**, 153–1580.
33. Reinhardt, P., Schmid, B., Burbulla, L.F., Schöndorf, D.C., Wagner, L., Glatza, M., Höing, S., Hargus, G., Heck, S.A., Dhingra, A., *et al.* (2013) Genetic correction of a LRRK2 mutation in human iPSCs links parkinsonian neurodegeneration to ERK-dependent changes in gene expression. *Cell Stem Cell*, **12**, 354–367.
34. Parisiadou, L., Xie, C., Cho, H.J., Lin, X., Gu, X.L., Long, C.X., Lobbestael, E., Baekelandt, V., Taymans, J.M., Sun, L. and Cai, H. (2009) Phosphorylation of ezrin/radixin/moesin proteins by LRRK2 promotes the rearrangement of actin cytoskeleton in neuronal morphogenesis. *J. Neurosci.*, **29**, 13971–13980.
35. Stafa, K., Trancikova, A., Webber, P.J., Glauser, L., West, A.B. and Moore, D.J. (2012) GTPase activity and neuronal toxicity of Parkinson's disease-associated LRRK2 is regulated by ArfGAP1. *PLoS Genet.*, **8**, e1002526.
36. Dusonchet, J., Li, H., Guillily, M., Liu, M., Stafa, K., Derada Troletti, C., Boon, J.Y., Saha, S., Glauser, L., Mamais, A., *et al.* (2014) A Parkinson's disease gene regulatory network identifies the signaling protein RGS2 as a modulator of LRRK2 activity and neuronal toxicity. *Hum. Mol. Genet.*, **23**, 4887–4905.
37. Yun, H.J., Kim, H., Ga, I., Oh, H., Ho, D.H., Kim, J., Seo, H., Son, I. and Seol, W. (2015) An early endosome regulator, Rab5b, is an LRRK2 kinase substrate. *J. Biochem.*, **157**, 485–495.
38. Kanao, T., Venderova, K., Park, D.S., Unterman, T., Lu, B. and Imai, Y. (2010) Activation of FoxO by LRRK2 induces expression of proapoptotic proteins and alters survival of postmitotic dopaminergic neuron in Drosophila. *Hum. Mol. Genet.*, **19**, 3747–3758.
39. Qing, H., Wong, W., McGeer, E.G.,. and McGeer, P.L. (2009) Lrrk2 phosphorylates alpha synuclein at serine 129: Parkinson disease implications. *Biochem. Biophys. Res. Commun.*, **387**, 149–152.
40. Bailey, R.M., Covy, J.P., Melrose, H.L., Rousseau, L., Watkinson, R., Knight, J., Miles, S., Farrer, M.J., Dickson, D.W., Giasson, B.I. and Lewis, J. (2013) LRRK2 phosphorylates novel tau epitopes and promotes tauopathy. *Acta Neuropathol.*, **126**, 809–827.
41. Ohta, E., Kawakami, F., Kubo, M. and Obata, F. (2011) LRRK2 directly phosphorylates Akt1 as a possible physiological substrate: impairment of the kinase activity by Parkinson's disease-associated mutations. *FEBS Lett.*, **585**, 2165–2170.
42. Hsu, C.H., Chan, D., Greggio, E., Saha, S., Guillily, M.D., Ferree, A., Raghavan, K., Shen, G.C., Segal, L., Ryu, H., *et al.* (2010) MKK6 binds and regulates expression of Parkinson's disease-related protein LRRK2. *J. Neurochem.*, **112**, 1593–1604.
43. Gloeckner, C.J., Schumacher, A., Boldt, K. and Ueffing, M. (2009) The Parkinson disease-associated protein kinase LRRK2 exhibits MAPKKK activity and phosphorylates MKK3/6 and MKK4/7, in vitro. *J. Neurochem.*, **109**, 959–968.
44. Mano, T., Suzuki, T., Tsuji, S. and Iwata, A. (2014) Differential effect of HDAC3 on cytoplasmic and nuclear huntingtin aggregates. *PLoS One*, **9**, e111277.
45. Häbig, K., Walter, M., Poths, S., Riess, O. and Bonin, M. (2008) RNA interference of LRRK2-microarray expression analysis of a Parkinson's disease key player. *Neurogenetics*, **9**, 83–94.
46. Schulz, C., Paus, M., Frey, K., Schmid, R., Kohl, Z., Mennerich, D., Winkler, J. and Gillardon, F. (2011) Leucine-rich repeat kinase 2 modulates retinoic acid-induced neuronal differentiation of murine embryonic stem cells. *PLoS One*, **6**, e20820.
47. Liu, Z., Lee, J., Krummey, S., Lu, W., Cai, H. and Lenardo, M.J. (2011) The kinase LRRK2 is a regulator of the transcription factor NFAT that modulates the severity of inflammatory bowel disease. *Nat. Immunol.*, **12**, 1063–1070.
48. Gardet, A., Benita, Y., Li, C., Sands, B.E., Ballester, I., Stevens, C., Korzenik, J.R., Rioux, J.D., Daly, M.J., Xavier, R.J. and Podolsky, D.K. (2010) LRRK2 is involved in the IFN-gamma

response and host response to pathogens. *J. Immunol.*, **185**, 5577–5585.
49. Kim, B., Yang, M.S., Choi, D., Kim, J.H., Kim, H.S., Seol, W., Choi, S., Jou, I., Kim, E.Y. and Joe, E.H. (2012) Impaired inflammatory responses in murine Lrrk2-knockdown brain microglia. *PLoS One*, **7**, e34693.
50. Hou, S.T., Jiang, S.X., Aylsworth, A., Cooke, M. and Zhou, L. (2013) Collapsin response mediator protein 3 deacetylates histone H4 to mediate nuclear condensation and neuronal death. *Sci. Rep.*, **3**, 1350.
51. Li, Y., Liu, W., Oo, T.F., Wang, L., Tang, Y., Jackson-Lewis, V., Zhou, C., Geghman, K., Bogdanov, M., Przedborski, S., *et al.* (2009) Mutant LRRK2(R1441G) BAC transgenic mice recapitulate cardinal features of Parkinson's disease. *Nat. Neurosci.*, **12**, 826–828.
52. Plowey, E.D., Cherra, S.J., 3rd, Liu, Y.J. and Chu, C.T. (2008) Role of autophagy in G2019S-LRRK2-associated neurite shortening in differentiated SH-SY5Y cells. *J. Neurochem.*, **105**, 1048–1056.
53. Ho, C.C., Rideout, H.J., Ribe, E., Troy, C.M. and Dauer, W.T. (2009) The Parkinson disease protein leucine-rich repeat kinase 2 transduces death signals via Fas-associated protein with death domain and caspase-8 in a cellular model of neurodegeneration. *J. Neurosci.*, **29**, 1011–1016.
54. Shin, N., Jeong, H., Kwon, J., Heo, H.Y., Kwon, J.J., Yun, H.J., Kim, C.H., Han, B.S., Tong, Y., Shen, J., *et al.* (2008) LRRK2 regulates synaptic vesicle endocytosis. *Exp. Cell Res.*, **314**, 2055–2065.
55. Heo, H.Y., Park, J.M., Kim, C.H., Han, B.S., Kim, K.S. and Seol, W. (2010) LRRK2 enhances oxidative stress-induced neurotoxicity via its kinase activity. *Exp. Cell Res.*, **316**, 649–656.